iScience

CellPress
OPEN ACCESS

Article

Developmental GAD2 Expression Reveals Progenitor-like Cells with Calcium Waves in Mammalian Crista Ampullaris

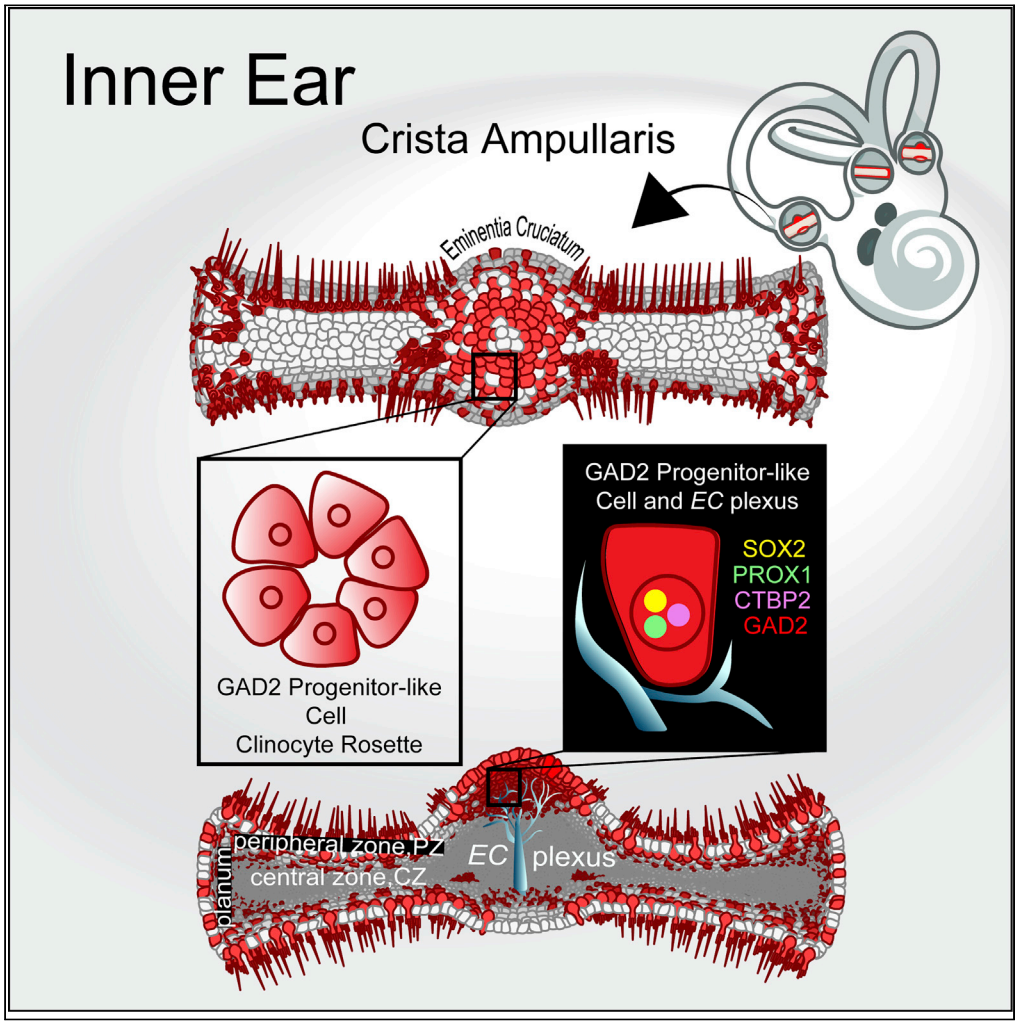

Holly A. Holman,
Yong Wan,
Richard D. Rabbitt

holly.holman@utah.edu

HIGHLIGHTS

ACh and muscarine evoke Ca^{2+} transients in GAD2 progenitor-like cells in mice

GAD2 progenitor-like cells form rosettes in neonates that are maintained in adults

Eminentia cruciata (EC) GAD2 cells express transcriptional factors SOX2, PROX1, CTBP2

A central *EC* structure, the *EC* plexus, branches out toward GAD2 progenitor-like cells

Holman et al., iScience *23*, 101407
August 21, 2020
https://doi.org/10.1016/j.isci.2020.101407

iScience

CellPress
OPEN ACCESS

Article

Developmental GAD2 Expression Reveals Progenitor-like Cells with Calcium Waves in Mammalian Crista Ampullaris

Holly A. Holman,[1,5,*] Yong Wan,[2] and Richard D. Rabbitt[1,3,4]

SUMMARY

Sense of motion, spatial orientation, and balance in vertebrates relies on sensory hair cells in the inner ear vestibular system. Vestibular supporting cells can regenerate hair cells that are lost from aging, ototoxicity, and trauma, although not all factors or specific cell types are known. Here we report a population of GAD2-positive cells in the mouse crista ampullaris and trace GAD2 progenitor-like cells that express pluripotent transcription factors SOX2, PROX1, and CTBP2. GAD2 progenitor-like cells organize into rosettes around a central branched structure in the *eminentia cruciatum (EC)* herein named the *EC* plexus. GCaMP5G calcium indicator shows spontaneous and acetylcholine-evoked whole-cell calcium waves in neonatal and adult mice. We present a hypothetical model that outlines the lineage and potential regenerative capacity of GAD2 cells in the mammalian vestibular neuroepithelium.

INTRODUCTION

Vestibular organs comprise one of the smallest and most complex sensory systems in gnathostomes orchestrating neural inputs from five organs, including three semicircular canals that provide a sense of linear and angular motion in three-dimensional space. Mechanotransduction takes place in specialized stereocilia projecting from the apical face of type I and type II sensory hair cells (HCs). The HCs in anterior and posterior semicircular canals sense rotation in the vertical plane. These cristae have a unique anatomical region in the center of their crista called the *eminentia cruciatum (EC)*, which is absent in the horizontal canal in most gnathostomes and not observed in adult primates. Electron microscopy studies described the *EC* in the anterior and posterior canals cotaining cells without cilia across several species including fish, turtles, birds, and mice (Igarashi and Yoshinobu, 1966; Igarashi and Alford, 1969; Harada, 1972, 1983; Collazo et al., 2005; Chagnaud et al., 2017). Lack of an anatomically distinct *EC* in primates and in the horizontal canals of other species resulted in a limited number of studies, leaving knowledge about cells located in the *EC*, their regulation, and physiological function(s) unknown.

In the crista and *EC*, cells lacking stereocilia are grouped as nonsensory supporting cells (SCs). When the crista is damaged, SCs begin to divide, which can lead to differentiation into either new HCs or new SCs in birds, fish, and mammals (Corwin and Cotanche, 1988; Ryals and Rubel, 1988; Forge et al., 1993; Warchol et al., 1993;Bermingham-McDonogh and Rubel, 2003; Brignull et al., 2009; Jiang et al., 2014; Cruz et al., 2015; Scheffer et al., 2015; Kniss et al., 2016; Slowik and Bermingham-McDonogh, 2016; Burns and Stone, 2017; Lush and Piotrowski, 2014, 2019; Wan et al., 2020). It is not known whether a specific population of SCs is responsible for regenerating HCs, SCs, or both in mouse cristae.

There is evidence that glutamic acid decarboxylase (GAD) is expressed in the SCs of mammalian cristae, although the specific physiological role remains uncertain. In a GAD67 transgenic mouse, SCs expressing GAD67-GFP were located primarily in the peripheral zone (PZ) of cristae (Tavazzani et al., 2014). In the PZ, afferent neurons predominantly make direct synaptic contacts with type II HCs via boutons instead of calyceal synapses with type I HCs in the central zone (CZ; Lindeman, 1969; Lim, 1976; Baird et al., 1988; Lysakowski and Goldberg, 1997; Fernández et al., 1998, 1995; Desai et al., 2005a), but it is not known what role SCs may play in synaptic transmission between HCs and afferent terminals or how GAD might be involved. Two GAD isoforms are responsible for synthesizing GABA, namely, GAD67 and GAD65, which are expressed from genes GAD1 and GAD2, respectively. In the central nervous system (CNS), GAD67

[1]Department of Biomedical Engineering, University of Utah, Salt Lake City, UT 84112, USA

[2]Scientific Computing and Imaging Institute, University of Utah, Salt Lake City, UT 84112, USA

[3]Graduate Program in Neuroscience, University of Utah, Salt Lake City, UT 84112, USA

[4]Department of Otolaryngology-Head & Neck Surgery, University of Utah, Salt Lake City, UT 84112, USA

[5]Lead Contact

*Correspondence: holly.holman@utah.edu

https://doi.org/10.1016/j.isci.2020.101407

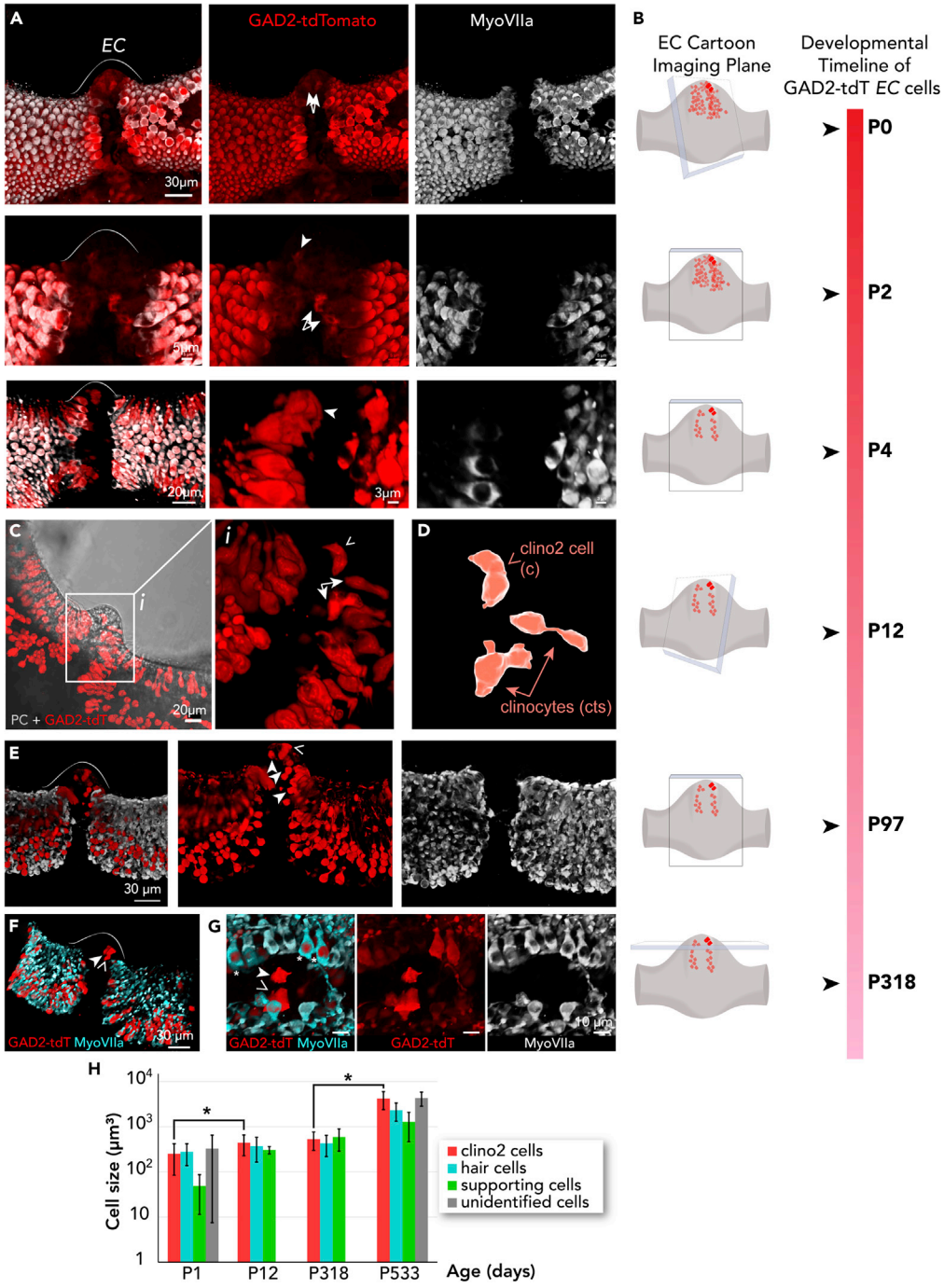

Figure 1. GAD2 Cells in *EC* and Crista

(A) Confocal microscopy of whole-mount fixed anterior canal cristae from transgenic mice (PC::G5-tdT), in the first postnatal week (A); day of birth (P0, k = 6), postnatal day 2 (P2, k = 3), and P4 (k = 5) with a GAD2 cell population (red) throughout the crista and hair cells (HCs) with MyoVIIa (white). Centrally located *EC* GAD2-tdT cells do not label with MyoVIIa (red; open arrowhead, clino2 cell; closed arrowheads, clinocytes).

(B) Illustrations are provided to orientate the plane in the corresponding confocal images.

(C) Phase contrast image overlaid with fluorescent confocal maximum intensity projection (MIP) gives relative position of GAD2-tdT cells throughout the crista and *EC* at postnatal day 12 (P12-14, k = 6). (i) Digitally zoomed ROI of the *EC* with an individual clino2 cell and clinocytes.

(D) Cell morphology and model rendering of a clino2 cell and two clinocytes (cts).

Figure 1. *Continued*
(E and F) The clino2 cell (open arrow) and cts (closed arrows) maintain their relative positions within the *EC* in adult mice (P97–P318, k = 12).
(G) A rotated view from (F) shows a clino2 cell (open arrow) and clinocyte (closed arrow) with surrounding HCs (cyan; MyoVIIa), and three HCs with GAD2-tdT (*).
(H) Average size of GAD2-tdT cells at different ages based ion segmentation with same relative size. Data are represented as mean ± SEM; *p < 0.05.

synthesizes GABA primarily for synaptogenesis, whereas GAD65 synthesizes GABA for neurotransmission (Kanaani et al., 1999). GAD67 is expressed during early development, whereas GAD65 is expressed at later ages, reflecting functional differences in each GAD isoform in the CNS (Esclapez et al., 1994; Bowers et al., 1998). These findings motivated analysis of GAD-positive SCs in the crista during postnatal development.

We examined vestibular neuroepithelium from the first filial generation of GAD2-IRES-Cre crossed with a dual reporter GCaMP5G-tdTomato line (Holman et al., 2019). In this study, GAD2-tdTomato (GAD2-tdT) cells were observed in the *EC* and specific zones within vertical cristae . Two unique GAD2-tdT *EC* cell types were identified based on their location within the *EC* and their ACh-evoked Ca^{2+} transients. During early postnatal development GAD2-tdT *EC* cells initially form mosaics that eventually organize into rosettes around an *EC* plexus, a core structure with extending branches in the middle of the *EC*. We report genetic and biochemical evidence for *EC* GAD2 progenitor-like cells with acetylcholine- and muscarine-evoked calcium waves reversibly blocked by atropine and 2-aminoethoxydiphenyl borate (2-APB) during postnatal development.

RESULTS

Tracking GAD2-tdT Cells in the Crista and *EC*

We hypothesized that a GAD2-IRES-Cre driver that targets astrocytes and GABAergic neurons in the CNS would similarly target GABAergic SCs in the semicircular canal cristae. GAD2-IRES-Cre driver was crossed with a dual GCaMP5G-tdTomato reporter line and whole mount cristae were examined. At day of birth, the earliest age examined in this study, GAD2-tdTomato (GAD2-tdT) cells were observed throughout the neuroepithelium (P0, Figure 1A). Illustrations in Figure 1B represent the optical imaging plane and age corresponding to the confocal images shown in Figure 1A. Representative whole-mount images of GAD2-tdT cells in cristae from ages P0 to P318 are shown (Figures 1A and 1C–1G). Immunolabeling with the HC marker MyoVIIa shows the location of developing HCs and a subpopulation of HCs with GAD2-dT in the first postnatal week. We observed an absence of MyoVIIa immunolabeling in the *EC* during development (Figure 1A) and in adults (Figures 1C and 1E–1G), further demonstrating a lack of HCs in the *EC*.

Two GAD2-tdT cell types with distinct locations are present in the center and slope (i.e., clino) of the *EC* and referred to as clinocytes and clino2 cells, respectively (arrows, Figures 1A, 1Ci, and 1D; Table 1). GAD2-tdT cells with similar morphologies located more internally within the *EC* are referred to as clinocytes (cts; Figures 1A, 1Ci, and 1D, filled arrows), whereas GAD2-tdT cells located on the edge of the *EC* with consistent and highly expressed tdT are referred to as clino2 cells (open arrow). During the second postnatal week GAD2-tdT *EC* cell boundaries are better defined (Figures 1C–F and 1G). In Figure 1C, phase contrast and fluorescence images are overlaid to visualize the size, shape, and position of the clino2 cell, clinocytes, and HCs in an anterior canal *EC* relative to the crista. Three-dimensionally reconstructed surfaces of the clino2 cell and clinocytes are shown (Figure 1D). Surface renderings of the clino2 cells and clinocytes

	Cell Description	Antigenic Phenotype
clinocyte	GAD2 progenitor-like cell, which organizes into rosettes in the *eminentia cruciata* (*EC*); located centrally in the *EC*.	SOX2, PROX1, CTBP2, GABA
clino2 cell	GAD2 progenitor-like cell located on the slope (i.e., clino), and edge of the *EC*.	SOX2, GABA

Table 1. Summary of GAD2 Progenitor-like Clinocyte and Clino2 Cell Features

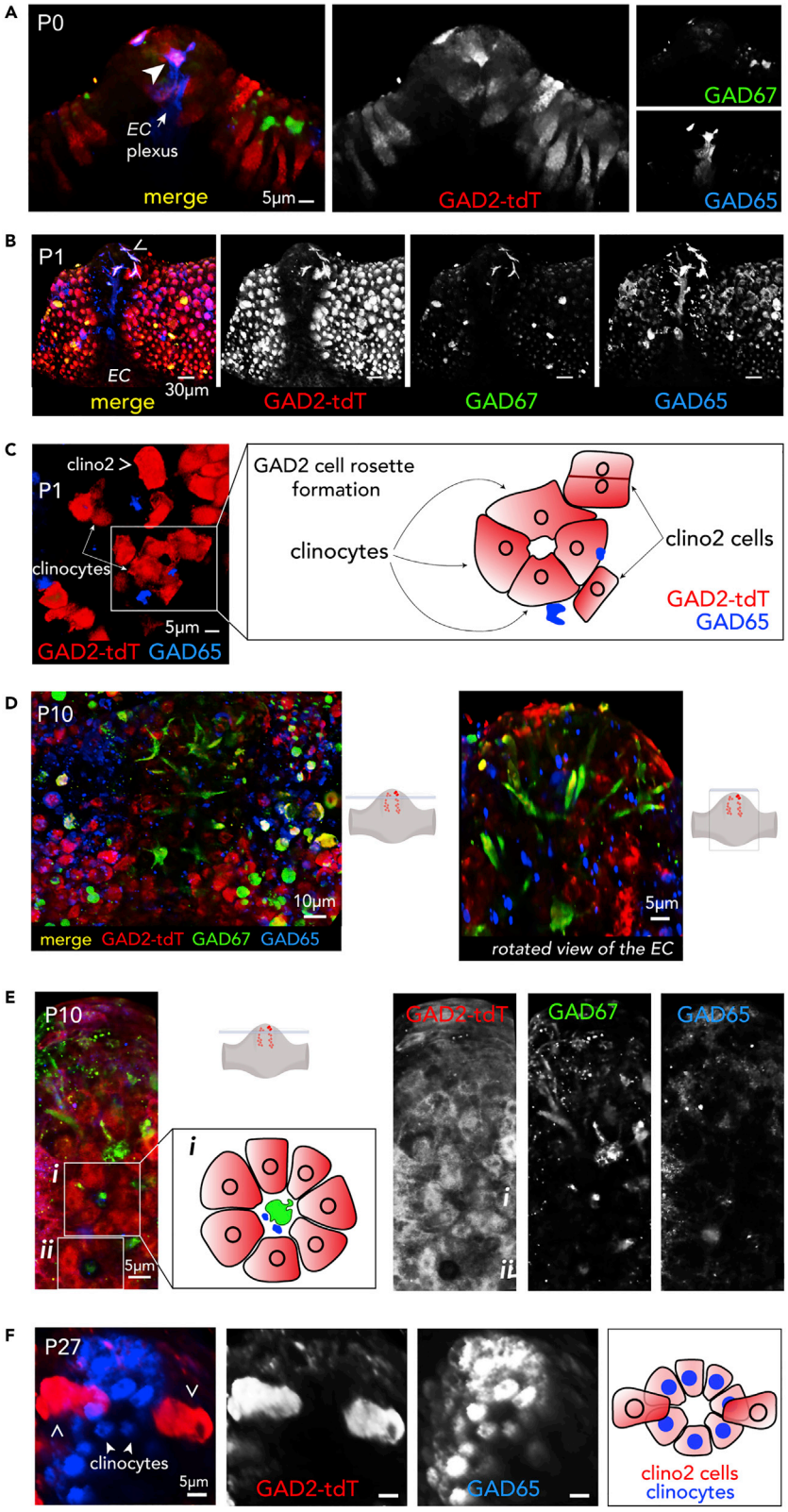
A
P0
EC
plexus
merge
5μm
GAD2-tdT
GAD67
GAD65
B
P1
EC
merge
30μm
GAD2-tdT
GAD67
GAD65
C
clino2 >
P1
clinocytes
5μm
GAD2-tdT GAD65
GAD2 cell rosette formation
clinocytes
clino2 cells
GAD2-tdT
GAD65
D
P10
10μm
merge GAD2-tdT GAD67 GAD65
5μm
rotated view of the EC
E
P10
i
ii
5μm
i
GAD2-tdT
GAD67
GAD65
F
P27
clinocytes
5μm
GAD2-tdT
GAD65
clino2 cells
clinocytes

Figure 2. Immunohistochemistry of GAD65 and GAD67 in the *EC*

(A) On day of birth, GAD65 (blue) co-labels GAD2-tdT cells (red; small arrow), and a central plexus structure in the *EC* (large arrow). Immunolabeling of GAD67 (green) occurs in cells on the side of the *EC* (k = 2).

(B) *EC* GAD2 cells with star-shaped morphologies along the edge of the *EC* at P1 label with GAD65 and GAD67. The central *EC* structure (*EC* plexus) labels with anti-GAD65 antibody (blue).

(C) At P1, clinocytes begin to form mosaics (k = 2). Clino2 cells (red) are adjacent to the clinocyte mosaic.

(D) At P10, the *EC* has many GAD2-tdT cells surrounding GAD65 and GAD67 puncta (k = 3). The image is rotated 90° on the x axis for visualizing GAD65, GAD67, and GAD2-tdT within the *EC*.

(E) Clinocytes (red) organize to form rosettes (i, ii) surrounding GAD65 (blue) and GAD67 (green) puncta at age P10 in the *EC*; (i) a cartoon depicting a clinocyte rosettes formation with GAD65 and GAD67 puncta in the center.

(F) A month old, a rosette with GAD65 puncta (blue, closed arrowhead) shows predominant GAD2-tdT expression in two opposing clino2 cells (red, open arrowhead) (P27-28, k = 3).

provide additional volume and cell morphology analysis (see Methods). Spatial relationships and volume ratio of the clino2 cell and clinocytes remain the same relative to the crista from neonate to adult ages (Figures 1D and 1H). In a mature mouse (P318), a subpopulation of GAD2-tdT HCs (red) persists among the HC population (cyan) in the crista with clinocytes and clino2 cells in the *EC* (Figure 1F). Figure 1G is a rotated 90° view of the *EC* visualizing the topology between a clino2 cell (open arrow) and clinocyte in the *EC* (closed arrow) relative to the GAD2-tdT HCs in the adjacent CZ (Figure 1G).

Average volumes of GAD2-tdT cells are shown in Figure 1H. Data are represented as mean ± SEM. Clino2 cells have an average volume of 1,408 μm^3 (4,180 voxels) (n = 1), clinocytes have an average volume of 1,172 μm^3 (3,273 voxels; n = 3), and GAD2-tdT HCs have an average volume size of 998 μm^3 (3,701 voxels; n = 4). clino2 cell volume increases proportionately to the crista with age; statistical analysis of P2 to P12 gives p values of $p < 0.098$ and between ages P318 and P533 $p < 0.082$. The close cell-to-cell junctions among clinocytes did not allow volume rendering or analysis of those cells.

GAD in the *EC*

To determine whether GAD2-tdT cells express glutamic acid decarboxylase, GAD65 or GAD67, immunohistochemistry was performed on cristae at different ages. GAD65 is present in the *EC* and co-labels clinocytes on day of birth (P0; blue, large arrow; Figure 2A). Immunolabeling with GAD65 reveals an additional structure in the middle of the *EC*, herein named *EC* plexus (small arrow). GAD67 expression is observed in cells near the *EC*, but does co-localize with GAD2-tdT cells or GAD65 at this age. By postnatal day 1 (P1), select clino2 cells at the edge of the *EC* co-label with GAD65 and GAD67 (arrow, Figure 2B). GAD65 immunolabelling regularly recognizes an *EC* plexus and labels branches extending outward toward clino2 cells and clinocytes.

One feature of clinocytes (red) is their ability to form multicellular mosaics with adjacent GAD65 puncta (blue, Figure 2C). In the second postnatal week, GAD65 and GAD67 co-label several branches of the *EC* plexus (P10, Figure 2D), and GAD65 uniquely labels additional puncta throughout the *EC*. A rotated view (right) is provided to visualize the extent of branching from the *EC* plexus (Figure 2D). By postnatal day 10, clinocytes form rosettes consisting of at least six cells with GAD65 and GAD67 puncta in the middle (Figure 2E, box). Due to the three-dimensional structure of the *EC*, visualization of multiple rosettes and branches from the *EC* plexus are not apparent (Figure 2D). A deep dive of datasets from multiple whole-mount tissues (z stacks) using image rendering techniques in FluoRender revealed rosettes from multiple cristae (k = 10). At age P27, clinocyte rosettes continued to form with GAD65 puncta in the center (Figure 2F). In this example, prominent tdT expression in two opposing clino2 cells are positioned 180° apart around a clinocyte rosette (cartoon, right panel). These two clino2 cells may represent a different stage in cell cycle and an exit from the rosette.

Pluripotent Transcription Factors and GABA in *EC* Cells

We examined protein markers in clinocytes to determine what factors may be contributing to the organization of rosettes. Immunohistochemistry with known pluripotent transcription factors SOX2, PROX1, CTBP2, and ATOH1 was performed on whole-mount fixed tissues. Several studies have shown that SOX2 plays a pivotal role in the expansion of progenitor cells and differentiation of HCs during development in cochlear and vestibular organs (Dabdoub et al., 2008; Neves et al., 2013; Kempfle et al., 2016; Puligilla and Kelley, 2017; Atkinson et al., 2018; Yang et al., 2019; Steevens et al., 2019; Wan et al., 2020; Dvorakova et al., 2020). We observed SOX2 expression in clinocytes and clino2 cells in the first postnatal week (P1, Figure 3A).

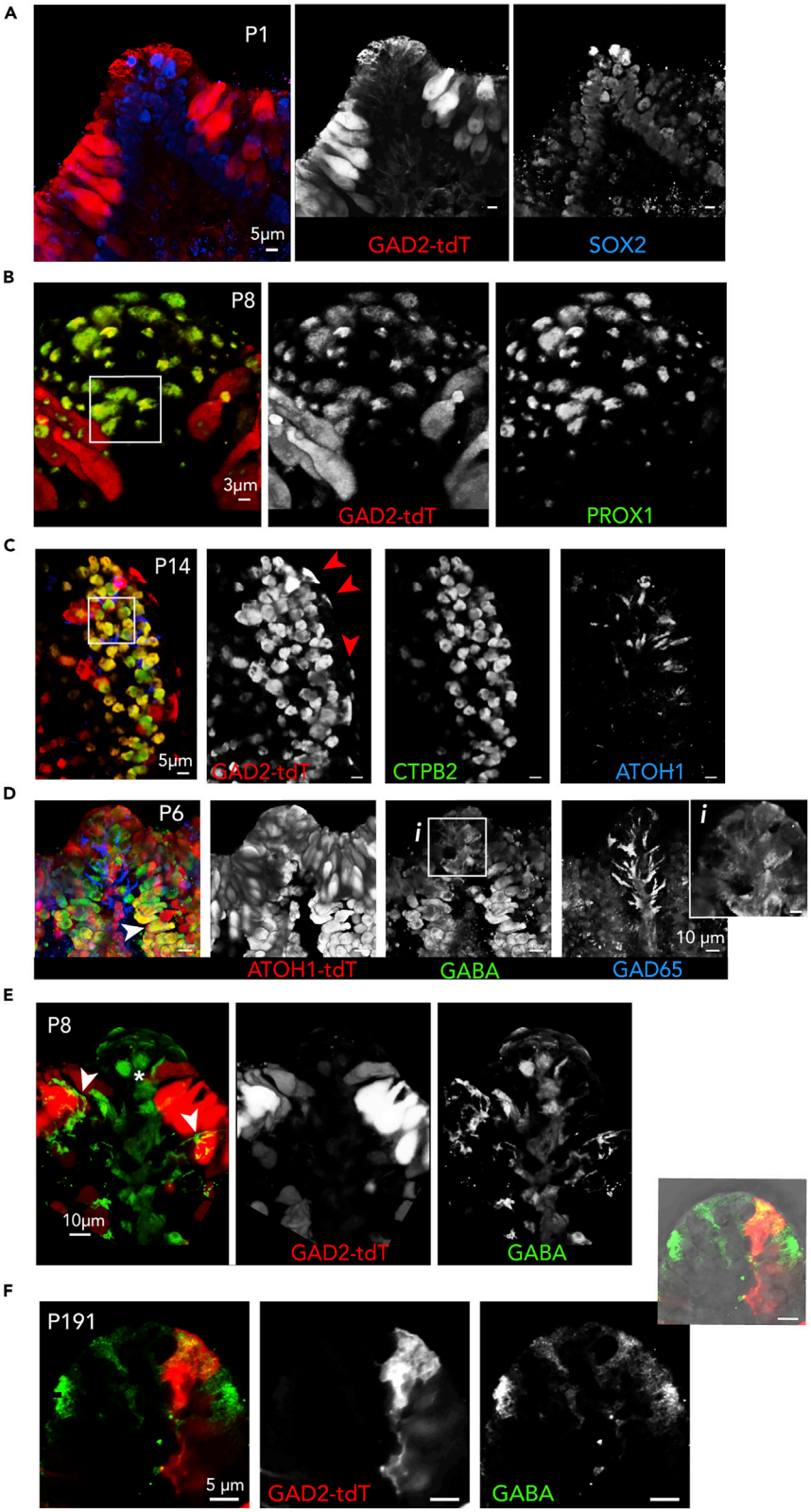
A
P1
5μm
GAD2-tdT
SOX2
B
P8
3μm
GAD2-tdT
PROX1
C
P14
5μm
GAD2-tdT
CTPB2
ATOH1
D
P6
ATOH1-tdT
i
GABA
i
10 μm
GAD65
E
P8
10μm
GAD2-tdT
GABA
F
P191
5 μm
GAD2-tdT
GABA

Figure 3. Clino2 Cells, and Clinocytes SOX2, PROX1, and CTBP2

(A) Immunolabeling of SOX2 in GAD2-tdT cells located in the central and distal regions of the *EC* shown in a 112-μm confocal z stack MIP (k = 2).

(B) Immunolabeling of PROX1 (green) in clinocytes (red) forming rosettes at age P8 (box; k = 1, n = 3 cristae).

(C) CTBP2 (green) co-localizes with clinocytes (red) forming rosettes (box). ATOH1 (blue) labeling is observed in the *EC* at P14, but does not colocalize with CTBP2 or GAD2-tdT (P5-14, k = 3).

(D) An ATOH1-Cre Tg with transgenic ATOH1 expression in *EC* cells (P6, k = 2). A population of *EC* cells label with GABA (green) in cells forming a rosette (i, box), whereas GAD65 (blue) labels the *EC* plexus. (i) Zoomed image of GABA-labeled cells forming rosettes; scale bar, 5 μm.

(E and F) (E) GAD2-tdT cells and *EC* cells not expressing GAD2-tdT label with GABA (green, star) during postnatal development (P6–P8, k = 2; E) and in adult mice (P191, k = 2; F). GABA also labels puncta close to GAD2-tdT cells on the sides of the EC (E, arrowheads) and beneath a clino2 cell in an adult mouse (F).

Another core transcription factor, PROX1, has been shown in SCs and HCs of the developing cochlear epithelium (Bermingham-McDonough and Rubel, 2003; Kirjavainen et al., 2008; Fritzsch et al., 2010; Liu et al., 2018). Clinocytes forming a rosette (box) also express PROX1 during postnatal development (Figure 3B).

At age P14 more rosettes are visible with clinocytes expressing the C-terminal binding protein 2 (CTBP2, green; Figure 3C, box). This multifunctional core CTBP2 protein plays an important role in HC ribbon synapses, whereas it is a transcriptional coregulator in other cell types. We report that CTBP2 is expressed in clinocytes, but not in clino2 cells located along the edges of the *EC*. This suggests an important transcriptional role for CTBP2 in these cells (arrows; red).

Previous lineage tracing of ATOH1 has demonstrated that it is crucial in the development of SCs and HCs in the organ of Corti, although it is not the only factor in determining HC fate (Fritzsch et al., 2005; Driver et al., 2013). Immunolabeling with an anti-ATOH1 antibody (blue, Figure 3C) showed ATOH1 in the *EC at P14*, but expression in clino2 cells or clinocytes was not observed. An ATOH1-Cre driver was used as a control to further test ATOH1 expression in the *EC*. The ATOH1-Cre driver was crossed with the same dual GCaMP5G-tdTomato reporter used in the GAD2-Cre cross. We observed ATOH1-tdT cells in the *EC* during early postnatal development at P6 (Figure 3D). Without a non-transgenic marker for clinocytes or clino2 cells at this time we are unable to confirm ATOH1 in clinocytes and clino2 cells. Using a polyclonal GABA antibody (A2052, Sigma), we observed GABA (green) in *EC* cells, including putative ATOH1-tdT HCs (arrow). With a monoclonal GABA antibody (A0310, Sigma), we observed GABA immunolabeling structures adjacent to GAD2-tdT HCs (red), and in putative synapses along the *EC* plexus (Figure 3E). Immunolabeling with GAD65 and GABA in the same tissue gave distinct patterns that often did not co-label, which may reflect a tight regulation of GAD65 or conformational changes of this enzyme (Kass et al., 2014).

In an adult mouse, GABA was present in a clino2 cell at the apex of the *EC* and in adjacent cells (P191, Figure 3F; GABA: A2052, Sigma). GABA puncta also appeared beneath the basolateral surface of the clino2 cell toward the *EC* plexus. A phase contrast overlay panel is provided for orientation of the *EC* (right).

ACh Evoked Ca^{2+} Transients in Clino2 Cells and Clinocytes

After characterizing GAD2-tdT expression patterns from neonates to old age mice, we imaged GCaMP5G (G5) to monitor calcium dynamics in these cells. Semi-intact vestibular organs were placed in a bath with continuous perfusion of media and imaged with swept field confocal microscopy (SFC). Puff application of 100 μM ACh and muscarine resulted in large G5 fluorescence modulation ($\Delta F/F_0$), whereas no detectable changes in G5 were observed from GABA application (100 μM; data not shown). Therefore, ACh- and muscarine-evoked calcium transients in GAD2-G5::tdT cells remained the focus of this study.

Figures 4A–4C reports the resting G5 fluorescence (F_0, blue) merged with peak changes in G5 ($\Delta F/F_0$, green). Spontaneous intracellular calcium transients appeared as waves with specific directionality from the apex of the cell closest to the cupula propagating toward the clino2 cell (c) base. Peak changes in GCaMP5G (G5) fluorescence during rest are shown in Figure 4B, $\Delta F/F_0$ (green), which were primarily seen in the clino2 cells (c), whereas G5 fluorescence changes in clinocytes were an order of magnitude smaller. A single 500-μs puff of 100 μM ACh evoked Ca^{2+} bursts in the clino2 cell (Figures 4A–4E) and clinocytes (Figures 4F–4I). These Ca^{2+} bursts started with a ~14 s latency and returned to baseline after approximately 90 s (Figures 4D–4J). In both clino2 cells and clinocytes, Ca^{2+} G5 fluorescence propagated

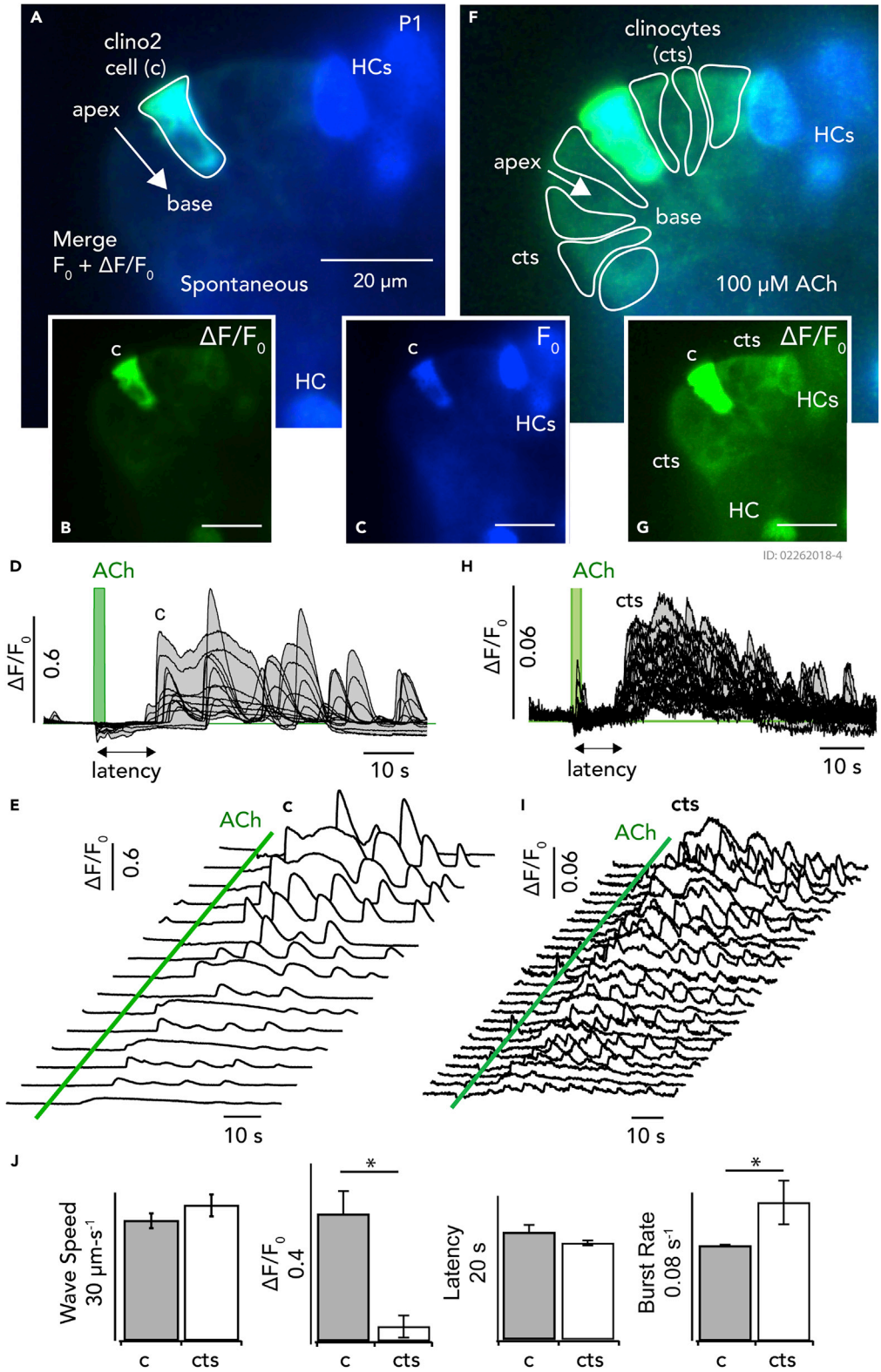

Figure 4. ACh-Evoked Calcium Transients in Clino2 Cells and Clinocytes at P1

(A–C) (A) Peak change in G5 fluorescence (B: $\Delta F/F_0$, green) merged with resting G5 fluorescence (C: F_0, blue) in the central region of the anterior canal crista.

Figure 4. *Continued*

(D and E) A 500-ms puff of 100 μM ACh triggered intracellular Ca^{2+} bursts in clino2 cells (c) with a latency of ~14 s and returning to baseline after ~90 s.

(F–I) Amplification of $\Delta F/F_0$ (green) revealed smaller ACh-evoked Ca^{2+} bursts in clinocytes (cts), occurring at faster rates. In both cell types (c and cts), Ca^{2+} initially increased at the apex of the cell facing the endolymph and traveled toward the base at a speed of ~25 μm-s^{-1}.

(J) Bar graphs show the wave speed, fluorescence intensity modulation, latency to the first ACh-evoked Ca^{2+} transient, and rate of evoked bursting (see Video S1). Data are represented as mean ± SEM; *$p < 0.05$.

as a wave from the apex to base at a speed of ~25 m/μs. Intracellular calcium wave speeds, G5 fluorescence intensity modulation, latency to the first ACh-evoked Ca^{2+} transient, and rate of evoked bursting were plotted for clino2 cells (c) and clinocytes (cts) (Figure 4J; also see Video S1). A significant difference of G5 fluorescence intensity modulation demonstrates that clino2 cells have a larger Ca^{2+} response compared with clinocytes (ΔF/F: clino2 cell = 0.29 ± 0.052; cts = 0.077 ± 0.0079). Furthermore, the burst rate in clinocytes at this postnatal age is significantly faster than in clino2 cells (rate: clino2 cell = 0.0534 ± 0.00054 s^{-1}; cts = 0.077 ± 0.0079 s^{-1}).

In Köllicker's organ and the organ of Corti, ATP activates purinergic receptors in surrounding SCs, inner HCs, and dendrites of primary auditory neurons (Glowatzki et al., 1997; Housley et al., 1998, 1999; Järlebark et al., 2000, 2002; Parker et al., 1998; Salih et al., 1999; Sueta et al., 2003; Szücs et al., 2004; Telang et al., 2010; Wang et al., 2003; Yan and Gu, 2013; Zhao et al., 2005; Chen et al., 1998). ATP can increase membrane conductance, cause rises in Ca^{2+}, and significantly change SC morphologies during development (Berekméri et al., 2019). Therefore, we tested the effects of ATP on possible purinergic signaling during development in clinocytes and clino2 cells. It was observed that 100 μM ATP evoked significant Ca^{2+} transients in multiple cell types in both the developing Köllicker's organ and organ of Corti, whereas there were no detectable ATP-evoked Ca^{2+} transients in clinocytes or clino2 cells of the same mouse (both ears were tested, data from one ear are shown; Figure S1 and Figure S2; Videos S1A and S1B).

Spontaneous Ca^{2+} Transients Evoked by ACh and Muscarine Blocked by Atropine

We next tested the effect of muscarinic receptor agonist atropine for its ability to block ACh- and muscarine-evoked Ca^{2+} transients in clino2 cells and clinocytes. Before ACh, muscarine, or atropine drug application two types of spontaneous Ca^{2+} events were observed and recorded (P1, Figures 5A–5C). One population of cells had slow spontaneous Ca^{2+} transients (Figure 5B, *c*) with a G5 fluorescence rise time constant of 2.80 ± 0.40 s, fall time constant of 17.1 ± 1.33 s, G5 half-width duration of 16.4 ± 1.35 s, ΔF/F 0.27 ± 0.020, and a frequency rate of 0.009 ± 0.0008 s^{-1}. Another cell population had fast spontaneous Ca^{2+} transients (Figure 5C, cts) with a G5 fluorescence rise time constant of 1.54 ± 0.080 s, G5 fall time constant of 2.87 ± 0.065 s, G5 half-width duration of 1.89 ± 0.055 s, ΔF/F 0.487 ± 0.033, and G5 frequency of 0.0256 ± 0.0026 s^{-1} (Figures 5F–5H). Muscarine (100 μM) evoked fast Ca^{2+} transients in clinocytes whereas clino2 cells had large and longer lasting Ca^{2+} transients (Figures 5D and 5E).

Sensitivity to a puff application of 100 μM ACh in the control condition (Figures 5I–K1) was blocked by 50 μM atropine (ATR; Figure 5K2) and partially recovered after washout (Figure 5K3). Relatively small ACh-evoked Ca^{2+} transients were also present in G5-expressing hair cells (HC) and their hair bundles (hb) (Videos S2, S3, S4A, and S4B).

Muscarine-Evoked Ca^{2+} Transients in Second Postnatal Week

To determine whether ACh- and muscarine-evoked Ca^{2+} transients persist through postnatal development we examined *EC* cells during the second postnatal week. ACh-evoked Ca^{2+} responses were observed where resting G5 fluorescence (F_0, blue) merged with peak changes in G5 fluorescence ($\Delta F/F_0$, green) recorded at two different focal planes (P10; Figure 6 Z_1(A), Z_2(B)). Short Ca^{2+} transients were evoked by 100 μM muscarine in clinocytes (cts) in focal plane Z_1, along with longer transients in clino2 cells (C; Figures 6A, 6C, and 6D). Clinocytes (cts) comprising the apex of the central crista and *EC* (focal plane Z_2) responded to muscarine with rapid Ca^{2+} transients (Figures 6B, 6E, and 6F). Kinetics of G5-detected Ca^{2+} transients were similar to those in P1 mice (c.f. Figure 3), but with reduced onset of latency (~6.5 s), fall (~1.45 s), half-width (~2.65 s), and frequency (~0.0385 s^{-1}) in the P10 compared with P1 tissues tested (Figures 6G and 6H; also see: Videos S5A and S5B). Data shown in Figure 6 are representative of muscarine-evoked Ca^{2+} transients from 3 mice at similar ages (P10, P14, and P15). At this age and in adult mice, clinocytes and clino2 cells continue to have spontaneous and ACh-evoked Ca^{2+} transients (Figure S3).

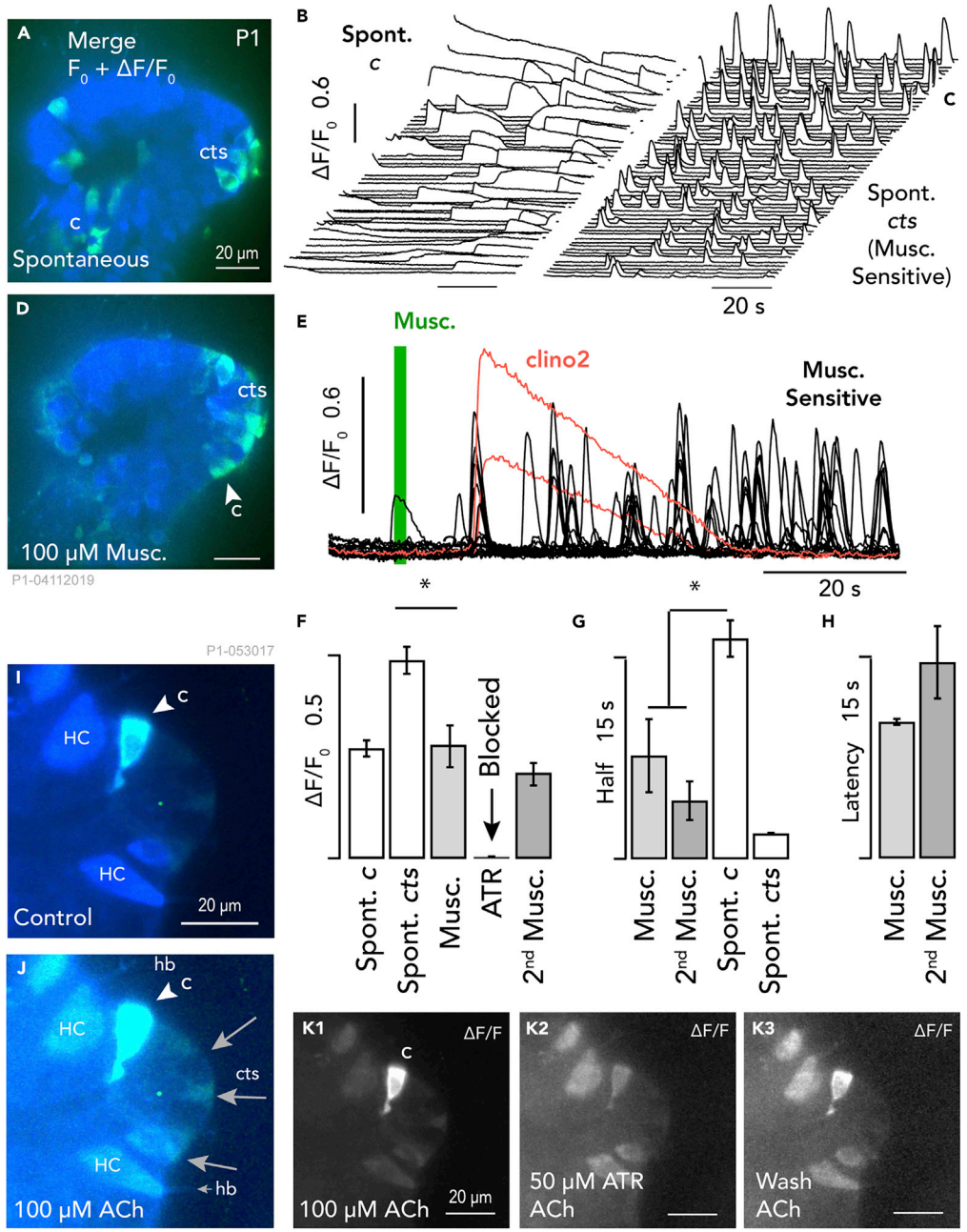

Figure 5. ACh- and Muscarine-Evoked Ca^{2+} Transients Blocked by Atropine at P1

(A) Resting G5 fluorescence (F_0, blue) merged with peak change in G5 fluorescence ($\Delta F/F_0$, green) occurring spontaneously in an excised preparation.

(B–E) (B and C) Waterfall plots of spontaneous Ca^{2+} transients in clino2 cells (*c*, n = 43; B and E–G), with long-lasting spontaneous transients, bursting in some cases (c.f. Figures 4 and 6). (C and E–G) Spontaneous Ca^{2+} transients in clinocytes (*cts*, n = 57) exhibited short events. (D and E) A 1-s puff of 100 μM muscarine evoked bursts of short Ca^{2+} transients in one cell population (*cts*, black traces), whereas another population had long-lasting Ca^{2+}increases (red traces).

(F–H) Muscarine evoked short Ca^{2+} transients in clinocytes and bursts of long-lasting transients in clino2 cells. Data are represented as mean ± SEM, *p < 0.05. (F–H) Spontaneous and muscarine-evoked Ca^{2+} transients in clino2 (c) and clinocytes (cts): (F) peak $\Delta F/F_0$, (G) event half-widths; (H) latency to first muscarine-evoked response. (F) Atropine (ATR) reversibly blocked responses to muscarine. (H) Latency to the first pooled muscarine-evoked Ca^{2+} transients before 50 μM ATR (Musc.) and after washout (Musc. second) was statistically indistinguishable.

Figure 5. *Continued*
(I–K) ACh-evoked Ca^{2+} transients in the control condition of a clino2 cell (c) and clinocytes (cts) at P1 were blocked by atropine (50 μM ATR, K2), and partially recovered after washout (K3). Relatively small ACh-evoked Ca^{2+} transients were also present in G5-expressing hair cells (HC) and their hair bundles (hb; also see Videos S2, S3, S4A, and S4B).

Horizontal Canal Ca^{2+} Transients in GAD2-tdT Cells

As the mouse horizontal canal does not have an anatomically distinct *EC*, we examined the horizontal canal crista for GAD2-tdT cells with a morphology similar to that of clinocytes and clino2 cells (Figures S4A–S4E). Horizontal canal cristae from two representative ages, P1 (Figures S4C and S4D) and P35 (Figures S4A, S4B, and S4E), show GAD2-tdT cells throughout horizontal cristae. G5 resting fluorescence in GAD2-tdT cells responded to ACh (100 μM) with large G5 $\Delta F/F_0$ transients consistent with calcium transients observed in clino2 cells of anterior and posterior cristae (Figures S4C and S4D). Other GAD2-tdT cells with low G5 resting fluorescence responded to ACh with brief Ca^{2+} transients consistent with clinocytes (E; see Videos S2A and S2B). This raises the possibility that clinocytes and clino2 cells might be present in horizontal canal crista and cristae from primates in the absence of an *EC* (F). Immunolabeling of horizontal canal cristae with the HC marker MyoVIIa (green) and neurofilament marker NF200 (blue) show several GAD2-tdT type I HCs with calyces (ages P5, top panel, and P6, bottom panel). Hypothetical clino2 cells and clinocytes cluster near the planum (arrow, P5).

2-APB Blocks ACh-Evoked Ca^{2+} Transients in Clino2 Cells and Clinocytes

The IP_3 receptor inhibitor 2-APB, which blocks the IP_3 receptor in frog HCs (Rossi et al., 2006) and store-operated intracellular Ca^{2+} transients (Bootman et al., 2002) was tested for its effects on Ca^{2+} transients in clinocytes and clino2 cells. A semi-intact preparation of an anterior crista from a P10 mouse revealed a clino2 cell (c; solid green outline) and hair cells (HCs) with low levels of G5 fluorescence at rest (F_0, blue, Figure 7A). Clinocytes (cts) showed low levels of resting G5 fluorescence in the same tissue (dotted outline, *EC* boundary, Figure 7A). A puff of 100 μM ACh evoked large Ca^{2+} transients in clino2 cells (c) and modest Ca^{2+} transients in clinocytes (Figures 7B and 7E). ACh-evoked Ca^{2+} transients were blocked with a single puff of 50 μM 2-APB in clinocytes and largely, but not completely, blocked in the clino2 cell (Figures 7C and 7F). The relative magnitude of ACh-evoked Ca^{2+} transients and extent of the 2-APB block is shown by merging Figures 7A–7C (Figure 7D). ACh-evoked Ca^{2+} transients in control conditions were sorted by evoked Ca^{2+} transient peak values, and in control conditions, were sorted by peak values plotted as waterfall charts (Figure 7E). The largest G5 fluorescence observed was from a clino2 cell with Ca^{2+} transients throughout the cell, starting in the apex (1), then middle (2), and finally base (3) of these cells (green, Figure 7E). Black traces represent multiple regions of interest in clinocytes and HC-calyx complexes. Application of 50 μM 2-APB significantly reduced ACh-evoked Ca^{2+} transients in all cells (Figure 7F). Responses in clino2 cells were significantly blocked by 2-APB (green; 1, 2, 3). Some HC-calyx complexes continued to show $\Delta F/F_0$ modulation evoked by ACh application, whereas other cells had small evoked short low-level Ca^{2+} transients appearing as spontaneous events unrelated to the ACh application (Figures 7C and 7F, arrows; also see Videos S6A and S6B).

Vesicular GABA Transporter in the *EC* and Crista

With large calcium responses to ACh and muscarine we examined the presence of vesicular transporter mechanisms for ACh and GABA in the *EC* of wild-type C57BL/6J and GAD2-IRES-Cre transgenic mice. Efferent neurons in the cristae utilize ACh as the primary transmitter; however, many studies have reported an absence of efferent innervation in the *EC*. Neither choline acetyltransferase (CHAT) nor vesicular acetylcholine transporter were observed in the *EC* (data not shown). Taken together, this suggests that the endogenous source of ACh acting on clinocytes and clino2 cells does not arise directly from efferent synaptic release. Although the application of GABA did not evoke detectable Ca^{2+} transients in clinocytes or clino2 cells, we observed GABA and vesicular GABA transporter (VGAT) in the *EC* (Figure 8). During early postnatal development small VGAT puncta (green) are present near clino2 cells (red) and in cells around the *EC* (Figure 8A). VGAT continued to label puncta at the sides of the *EC* (P10, Figure 8B). The majority of VGAT immunolabeling appeared in puncta surrounding putative GAD2-tdT HCs in the crista (Figure 8C). In this example, four putative GAD2-tdT type I HCs align in a row within the crista (dotted box). When the boxed image is rotated (i) three putative GAD2 type I HCs are apparent with several surrounding VGAT puncta (2–4), presumably from synaptic contacts; one putative HC without GAD2-tdT is outlined with VGAT puncta (*). A GAD2-tdT cell with an SC morphology is devoid of synaptic VGAT puncta (red; 1). To verify the VGAT immunolabeling in GAD2-tdT transgenic mice we examined aged-matched wild-type C57BL/6J cristae. We observed VGAT puncta (green) near the apex and cuticular plates of cells (P8, Figure 8D). GAD65 puncta were present at the cell membranes in the apical, middle, and basolateral

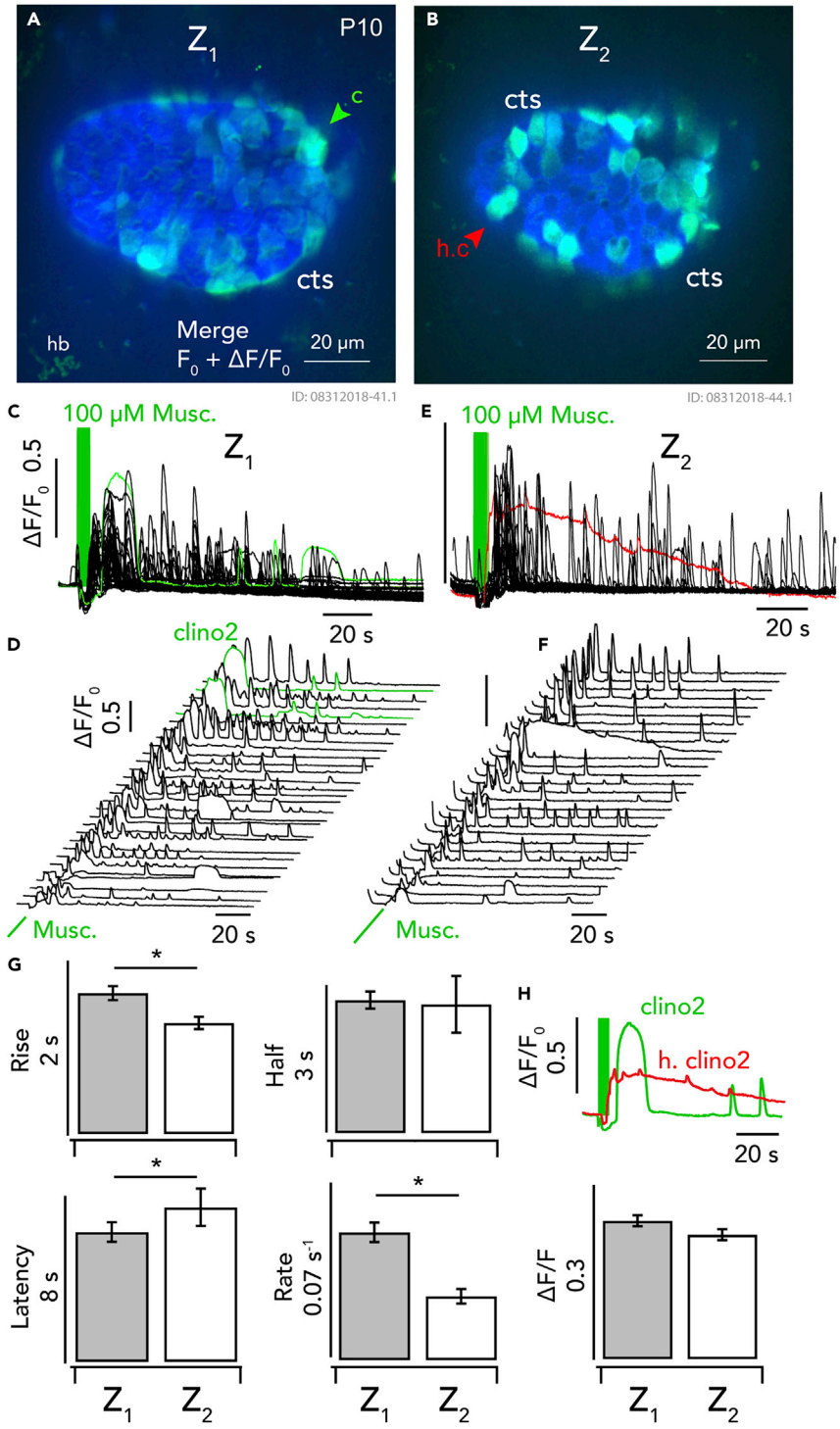

Figure 6. Muscarine-Evoked Ca^{2+} Transients at P10

(A and B) Resting G5 fluorescence (F_0, blue) merged with peak change in G5 fluorescence ($\Delta F/F_0$, green) evoked by 100 μM muscarine at two different focal planes (Z_1, Z_2) in the anterior crista.

(C and D) Short Ca^{2+} transients were evoked by muscarine in clinocytes (cts) in focal plane Z_1, and longer sustained or bursting transients in clino2 cells (c).

(E and F) (E) Clinocytes (cts) covering the apex of the central crista (focal plane Z_2) responded to muscarine with rapid Ca^{2+} transients. Transients are sorted by peak values for focal plane Z_1 (D, n = 29) and focal plane Z_2 (F, n = 28).

Figure 6. *Continued*
(G) Kinetics of G5-detected Ca^{2+} transients were similar to those in P1 mice (c.f. Figure 3), but with reduced onset latency in P10. Data are represented as mean ± SEM; *p < 0.05. H) A clino2 cell (clino2, green) and hypothetical clino2 cell (h. clino2, red) from Z_1 and Z_2 with different muscarine evoked Ca^{2+} transients (from graphs C and E).
(also see: Videos S5A and S5B).

regions (blue). A large GAD65 foci also was observed (*). These data further demonstrate that immunolabeling with GAD65 may not reflect all GABA activity.

ACh-Evoked Ca^{2+} Transients in *EC* GAD2 Progenitor-like Cells in Mature Mice

Previous studies have shown that C57BL/6J mice have age-related hearing loss (Ison et al., 2007; Mock et al., 2016), but the vestibular function in these mice is normal (Jones et al., 2006). Because C57BL/6J mice have a decline in cochlear function with age we examined whether clino2 cells and clinocytes maintained ACh- and muscarine-evoked Ca^{2+} transients in old age. Semi-intact vestibular organs were placed under SFC for live cell imaging with continuous perfusion. Resting G5 fluorescence (F_0, blue) merged with peak changes in G5 fluorescence ($\Delta F/F_0$, green) evoked by either 100 μM ACh (Figure 9A) or 300 μM muscarine (Figure 9B) in an anterior crista from a 2-year-old mouse (P825) was recorded. In this tissue clinocytes had three distinct ACh-evoked Ca^{2+} transients (1, 2; green traces, and 3, red trace). Responses in clinocytes were nearly identical between ACh and muscarine treatments (Figures 9A-9C and 9E-9G). Putative calyces (N) in the sensory HC domain of the crista (Figure 9A) responded to 100 μM ACh in mature mice with long-lasting Ca^{2+} transients (Figure 9D) consistent with previous studies examining mAChRs in calyces (Holt et al., 2017). The latency to the first evoked Ca^{2+} transient in this mouse was equivalent to that observed at P10 (c.f. Figure 4), suggesting that clinocytes are fully functional by age P10. Statistically significant differences between ACh and muscarine were recorded in the G5 fluorescence half-life, but the dose was not titrated to match strengths of the stimuli (Figure 9H; also see Videos S7A and S7B). The ACh-evoked Ca^{2+} transients in this mature mouse were apparent rhythmic bursts; however, bursting was also observed in clino2 cells and clinocytes in younger mice (e.g., Figure 6), ruling out age as a required factor. It has been suggested that small changes in IP_3 signaling in astrocytes can lead to highly diverse intracellular calcium events ranging from a solitary pulse to rhythmic bursts (Taheri et al., 2017), and it is possible that similar mechanisms are present in clino2 cells and clinocytes. It is not yet known if bursting or the precise temporal waveform plays an important role in the physiological function of these cells.

EC Plexus

Just below clino2 cells and clinocytes is a distinct anatomical structure with unknown function, denoted here as the *EC* plexus. To characterize the plexus, immunolabeling of CHAT, muscarinic acetylcholine receptor 1 (M1), and βIII tubulin (TUBB3) antibodies was tested. CHAT and M1 antibodies did not recognize epitopes within the *EC* (data not shown). Labeling with a fluorescently conjugated βIII tubulin antibody revealed a putative afferent fiber close to the *EC* (Figure 10A, inset, i). This βIII tubulin fiber appeared to initiate from one side of the crista, but was not observed within the *EC*, providing further evidence that the *EC* region is largely devoid of neurons. A split fluorescent image is shown of TUBB3-labeled afferent calyces (right side) and GAD2-tdT cells (left side) of a crista. This experiment was repeated in three mice from two age groups young (P0–P14) and mature (P100–P720), and βIII tubulin was consistently absent from the *EC* plexus. In Figure 10B, GAD65 immunolabels the *EC* plexus in a mature mouse aged P602 (Figure 10B), suggesting a functional relevance of the plexus throughout life. A mature mouse revealed individual clinocytes (arrows) contacted by branches from the *EC* plexus, along with the clino2 cell (*) at the *EC* periphery. Although GABA did not evoke detectable Ca^{2+} transients in clinocytes or clino2 cells with the current transgenic model, we tested an anti-$GABA_A$ receptor antibody as it has been shown to play a role in regulating neural progenitor cells via GABA signaling (Wang et al., 2003). Immunolabeling of $GABA_A$ receptor ($GABA_A$ R, blue) appears in structures surrounding the outer membrane of clinocytes (arrows) and a clino2 cells (star) in a mature mouse (P936; Figure 10C; also see Video S8). Immunolabeling with $GABA_A$ R also appears in puncta surrounding HCs (white, MyoVIIa) in the crista during postnatal development (P6, Figure 10D).

DISCUSSION

We show here that GAD2 progenitor-like cells in the *EC* of vertical semicircular canal cristae are present in neonates and maintained in adult mice. ACh and muscarine evoke atropine-sensitive Ca^{2+} transients that distinguish two GAD2 progenitor-like cell types: clinocyte and clino2 cell. Our data provide evidence for a role of GAD2 during development in the neuroepithelium of cristae and GAD2 progenitor-like cells in the *EC* forming contacts with a central *EC* structure, the *EC* plexus.

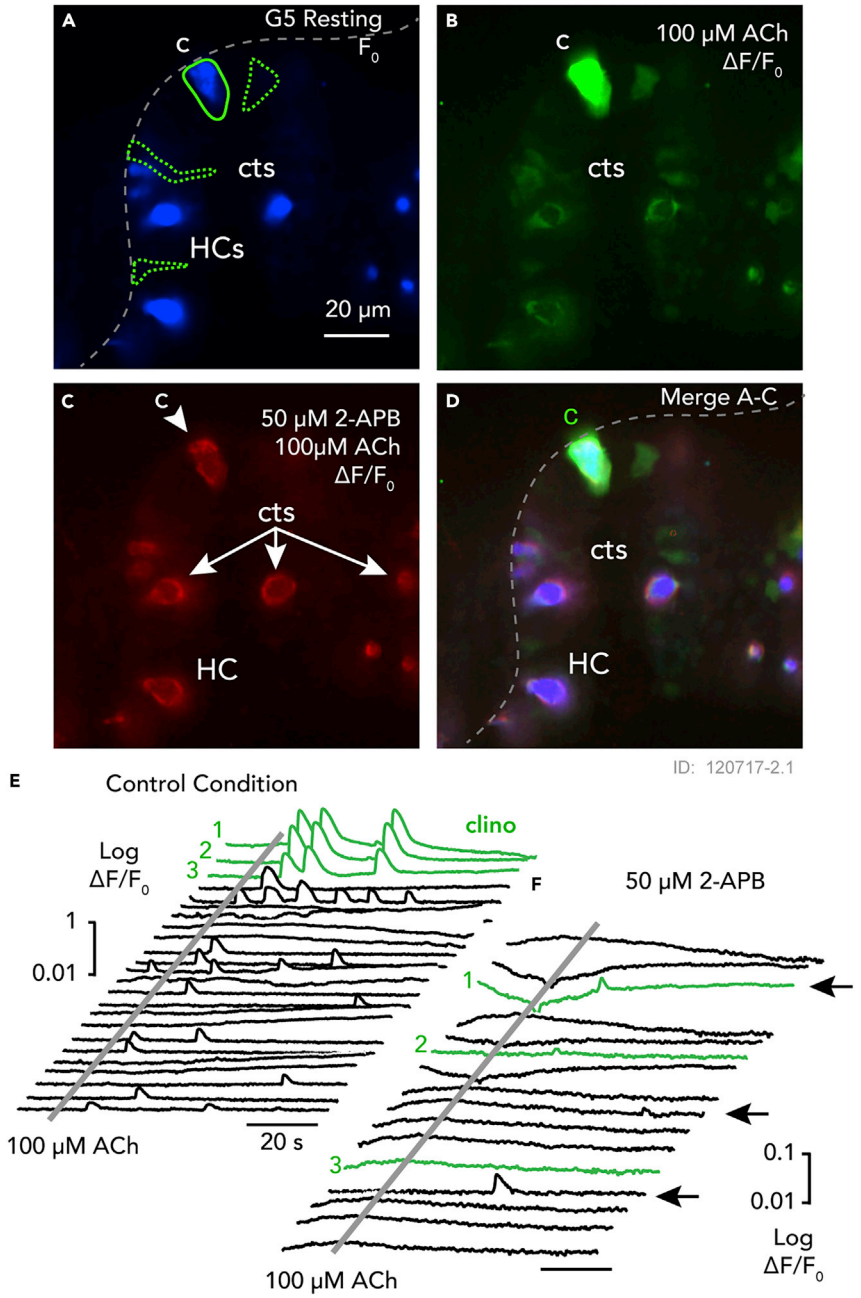

Figure 7. Blocking Action of 2-APB on ACh-Evoked Ca^{2+} Transients in the Anterior Crista at P10

(A) Clino2 cell (solid green outline) and hair cells with G5 fluorescence at rest (F_0, blue), whereas clinocytes (supporting, dotted green outlines) exhibit very modest G5 fluorescence at rest.

(B) ACh (100 μM) evokes intense Ca^{2+} transients in clino2 cell (c), and modest transients in clinocytes.

(C) ACh-evoked transients were blocked by 50 μM 2-APB in clinocytes and largely blocked in the clino2 cell.

(D) Relative magnitude of ACh-evoked transients and extent of 2-APB block is illustrated by merging (A–C).

(E) ACh-evoked transients in the control condition sorted by peak values. The largest transients were in the clino2 cell, with Ca^{2+} transients in the apical (1), central (2), and basal (3) regions of the cell (green). Black traces are clinocytes and hair cell–calyx complexes.

(F) Same cells as (E) in the presence of 50 μM 2-APB shown on a ~10× log scale. Responses in clino2 cells were largely blocked by 2-APB (green: 1, 2, 3). Some HC-calyx complexes continued to have low-frequency $\Delta F/F_0$ modulation following ACh application, whereas other cells had brief Ca^{2+} transients that appeared to be spontaneous (F: arrows) (also see Videos S6A and S6B).

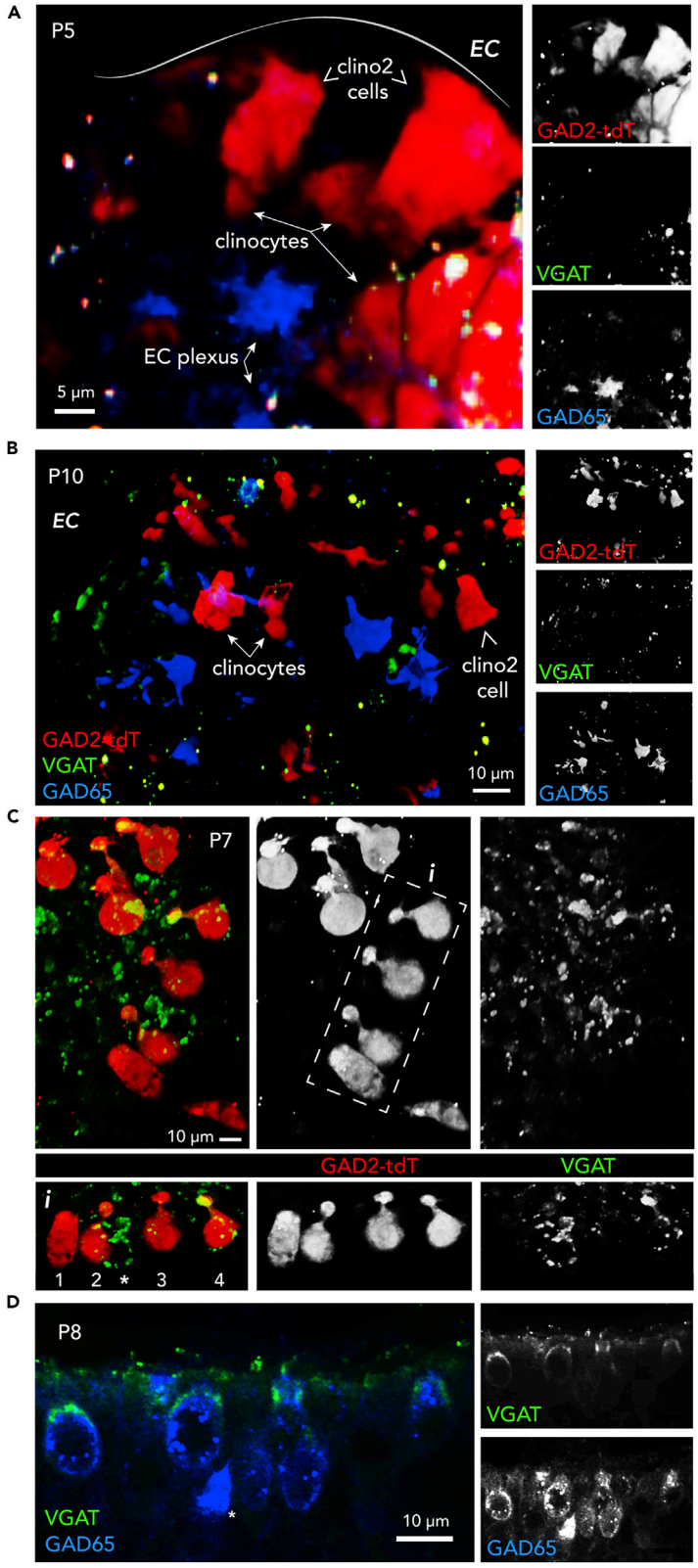
A
P5
EC
clino2 cells
clinocytes
EC plexus
5 µm
GAD2-tdT
VGAT
GAD65
B
P10
EC
clinocytes
clino2 cell
GAD2-tdT
VGAT
GAD65
10 µm
C
P7
10 µm
i
GAD2-tdT
VGAT
1 2 * 3 4
D
P8
VGAT
GAD65
10 µm

Figure 8. Vesicular GABA Transporter (VGAT) in the Crista not *EC*

(A) VGAT (green) co-labels with GAD65 (blue) in small puncta in the *EC* near clinocytes (red; P5–P7, k = 2). GAD65 also labels large central regions in the *EC* plexus.

(B) A top-down view of clinocytes (red) in the middle and a clino2 cell on the edge of the *EC* (P8–P10; k = 2).

(C) In the crista, VGAT puncta surround GAD2-tdT HCs (box, i). A row of 4 GAD2-tdT cells appear as 3 putative type I HCs (2–4) and a putative SC (left). The GAD2-tdT cells (2–4) have VGAT puncta around cell surfaces. The GAD2-tdT cell (1) with a different morphology lacks VGAT puncta.

(D) In a cross section of a crista, VGAT puncta are present near the apex of cells labeled with GAD65 puncta (blue), near the cell membrane. An extracellular structure also labeled with GAD65 (star).

GAD2 Progenitor-like Cells and Rosettes

Formation of multicellular rosettes occurs in many organs and species including zebrafish lateral line primordium, the *Drosophila* epithelium and retina, and adult neural stem cell niches (Mirzadeh et al., 2008; Elkabetz and Studer, 2008). To date, two mechanisms of cytoskeletal rearrangements have been described for rosette formation: apical constriction and planar polarized constriction (Harding et al., 2014). Extracellular cues that trigger these rearrangements *in vivo* are less well known and potentially more diverse.

In the CNS, neural precursor cells form rosettes in the ventral subventricular zone (V-SVZ) and act as a niche for neural stem cells, giving rise to specific subtypes of olfactory neurons and glial cells (Merkle et al., 2007; Goldberg and Hirschi, 2009; Giachino et al., 2014a,2014b). Unlike the transient embryonic rosettes seen in many systems, V-SVZ rosettes are maintained throughout adulthood, although there is a decrease in the number of rosettes with age (Shook et al., 2012). These rosettes provide a niche environment for proliferation and differentiation of adult neural stem cells.

V-SVZ rosettes are composed of ependymal cells that contact the cerebrospinal fluid of the ventricle surface and astrocyte-like cells that contact blood vessels (Ihrie and Alvarez-Buylla, 2011; Fuentealba et al., 2012). Clinocytes may hypothetically contact both the cupula and the surface of the *EC* plexus. This previously undescribed structure located in the center of the *EC* resembles a ventricle with its location, immunolabeling, and significant branching. The *EC* plexus may provide signaling mechanisms similar to the V-SVZ region described above and in other CNS regions (Tochitani and Kondo, 2013). Future studies examining the cellular composition and physiology of the plexus will determine its function.

Clinocytes and Clino2 Cells: GAD2, SOX2, PROX1, and CTBP2

Several studies have reported the important role of SOX2 in the organ of Corti during development (Dabdoub et al., 2008; Gu et al., 2016; Cheng et al., 2019; Kempfle et al., 2016; Yang et al., 2019; Locher et al., 2013; Wilkerson et al., 2019; Neves et al., 2013; Kiernan et al., 2005; Dvorakova et al., 2020). Similarly, SOX2 plays a vital role in the development of SC and HCs in the vestibular system. We demonstrate that clinocytes and clino2 cells express SOX2 during early postnatal development. Examining additional pluripotent factors including the stem cell marker Lgr5 and the Notch/Wnt signaling molecules would provide further insight into the mechanisms of these cells.

The transcription factor PROX1 is induced and regulated by SOX2 and is essential for controlling crista size (Dabdoub et al., 2008; Liu et al., 2018; Fritzsch et al., 2010). In this study, we observed PROX1 in clinocytes at a single age (P8); however, further studies are required to determine its potential regulatory mechanism in these cells.

CTBP2 is a transcription factor that has been less studied for its potential role in transcriptional regulation in cells of the vestibular epithelium. This is likely because of the significant role that CTPB2 plays in HC ribbon synapses. CTBP2 contributes to cell fate in mouse embryonic stem cells (mESCs) through the Oct4-interacting proteins, suggesting that CTBP2 is necessary for Oct4 function in establishing ESC identity (Ding et al., 2012; Tapia et al., 2015; van den Berg et al., 2010; Kim et al., 2015). Cells lacking CTBP2 have demonstrated delays in differentiation (Tarleton and Lemischka, 2010). Other studies report that CTBP2 acts as a transcriptional repressor facilitating the Notch signaling pathway (Suh et al., 2018). Published data suggest the presence of diffuse CTBP2 immunolabeling in mouse inner HC nuclei and adult mouse Lgr5 cell colonies (Kujawa and Liberman, 2009; Sergeyenko et al., 2013; McLean et al., 2017). Future studies examining the role of CTBP2 in clinocyte regulation would enhance our understanding of these cells and may provide information for the differential gene expression among clinocytes and clino2 cells.

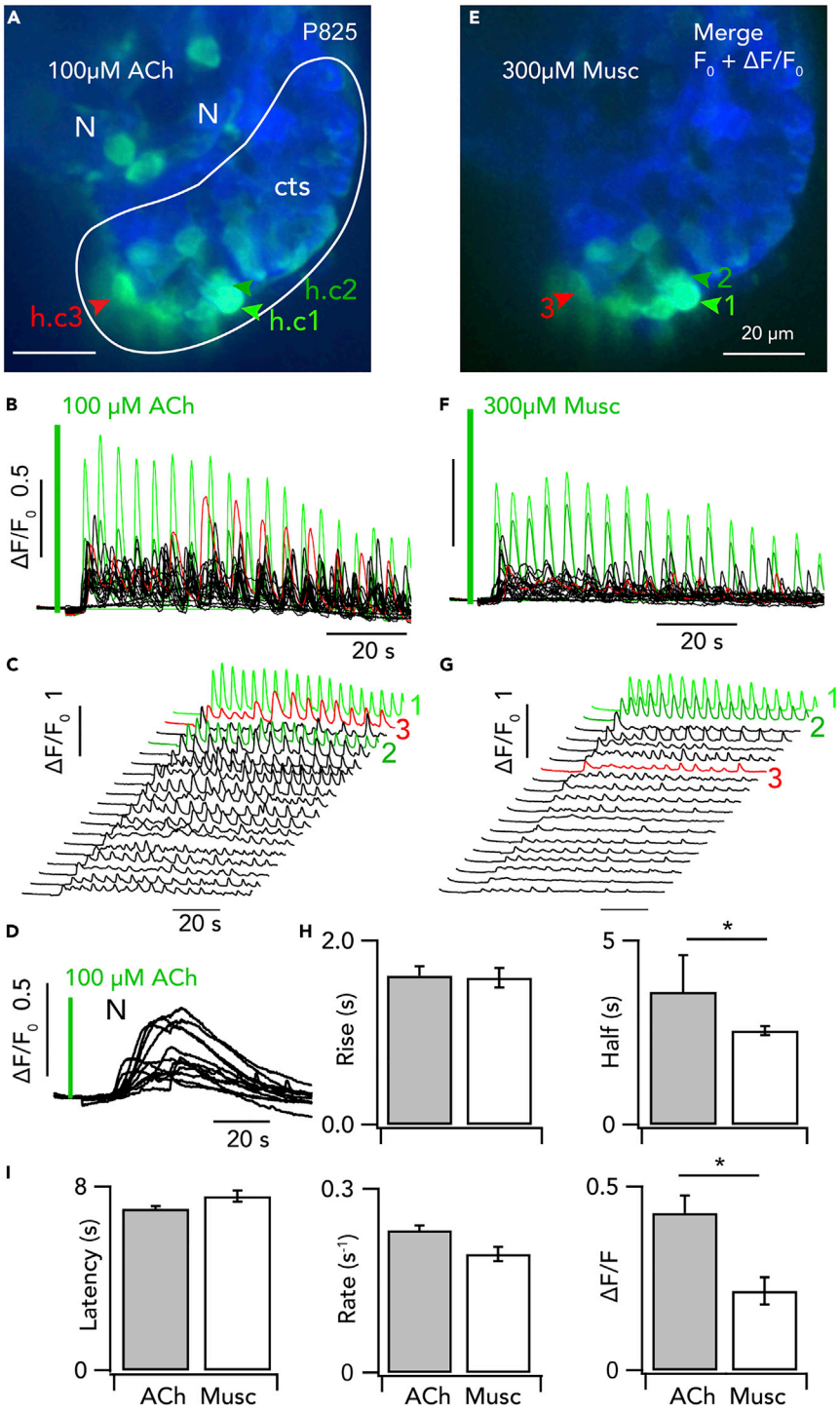

Figure 9. ACh- and Muscarine-Evoked Ca^{2+} Transients in Clinocytes in Mature Mice

(A and B) Resting G5 fluorescence (F_0, blue) merged with peak change in G5 fluorescence ($\Delta F/F_0$, green) evoked by 100 μM ACh (A, n = 19) and in the same cells 300 μM muscarine (B, n = 19) in the anterior crista of a P825 mouse. (C–G) Clinocytes responses were nearly identical between ACh and muscarine treatments. (D) Putative calyces (N, n = 12) in the sensory hair cell domain of the crista (A) respond to 100 μM ACh in adult mice with long-lasting Ca^{2+} transients distinct from those evoked by muscarine or ACh in clinocytes. Latency to the first calcium transient in adult and mature mice was similar to that observed at P10 (c.f. Figure 4), suggesting that clinocytes are fully functional by P10.

Figure 9. *Continued*
(H and I) Bar graphs quantify the evoked Ca^{2+} transientsfrom ACh (grey) and muscarine (Musc., white)Data are represented as mean ± SEM; *p < 0.05. (I) The latency of evoked Ca^{2+} transients and rates of evoked Ca^{2+} transients after ACh or Musc were not signifianctly different, but peak changes in G5 fluorescence ($\Delta F/F_0$) was dignificantly less in Musc (also see: Videos S7A and S7B).

We propose a hypothetical model for the *EC* GAD2 progenitor cell lineage where clinocytes (CTs) organize into rosettes in a quiescent state (Figure 11). Expression of GAD2 in CTs leads to GABA synthesis with SOX2 and unknown transcription factors (TF_1). GABA along with other signaling molecules (SM_1) signals back to CTs, promoting their self-renewal. If GABA synthesis is reduced or blocked, proliferation of CTs may undergo cell division and differentiate into clino2 cells (CC) with SOX2 with additional transcription factors (TF_2) and signaling molecules (SM_2). Transcriptional regulation in clino2 cells (TF_3) and signaling to clino2 cells (SM_3) may promote division into SCs, and further differentiation to GAD2 HCs (TF_4) with other signaling molecules (SM_4).

GABA and ACh Signaling

GABA is a conserved signaling molecule and adapted to serve as the predominant inhibitory neurotransmitter in the CNS. In the adult hippocampus SGZ neurogenic niche of radial-like glial cells maintains quiescence by tonic GABA release from interneurons. Once interneurons differentiate into neural progenitor cells, GABA continues to regulate their development into mature granule cells (Jin et al., 2001; Tozuka et al., 2005; Coulter and Carlson, 2007; Houser, 2007; Kim et al., 2012; Catavero et al., 2018). As clino2 cells have detectable levels of GABA and the *EC* plexus immunolabels with $GABA_A$ R we hypothesize that similar signaling mechanisms may contribute to proliferation of clinocytes and differentiation into clino2 cells in the *EC* (Figure 11). Further lineage tracing and single-cell analysis of *EC* GAD2 cells would provide information on the temporal control of GAD2 in clinocytes and clino2 cell progeny.

We demonstrate the presence of GABAergic machinery in the *EC*; however, many functional questions remain. Given the muscarinic ACh-evoked Ca^{2+} transients reported here, we hypothesize that ACh may modulate non-vesicular GABA released by clinocytes and clino2 cells and provide a mechanism for signaling to the *EC* plexus. The absence of innervation in the *EC* is consistent with previous reports (Desai et al., 2005a, 2005b; Lysakowski, 1996), and a source for ACh in the *EC* remains unknown. Evidence from other systems suggests that ACh plays a role in local cell signaling and autocrine function in embryos and adults (Grando, 1997; Wessler et al., 1998, Wessler and Kirkpatrick, 2008; Williams et al., 2004). Non-neuronal mouse and human embryonic stem cells express CHAT and muscarinic ACh receptors (Serobyan et al., 2007; Paraoanu et al., 2007a,2007b; Landgraf et al., 2010; Takahashi et al., 2014), and in mice, ACh mobilizes Ca^{2+}, which increases cell viability, decreasing cell proliferation.

Although previous studies determined an *EC* in phylogenetically diverse species including birds, fish, frogs, turtles, bats, cats, dogs, rats, and mice (Igarashi and Yoshinobu, 1966; Lewis et al., 1985; Fritzsch et al., 2002), an *EC* has not been observed in all mammals. One possibility is that cell types identified here in the *EC* of mice are present, but not organized in an anatomically distinct *EC*. Based on this, further examination of GAD2, GABA, and the *EC* including clinocytes, clino2 cells, and the *EC* plexus is necessary to determine whether there are equivalent cells and mechanisms in human and non-human primates.

Limitations of the Study

This study utilized transgenic mice with a C57BL/6 strain of origin (Taniguchi et al., 2011; Gee et al., 2014). Previous studies reported C57BL/6 mice with early-onset hearing loss (Ison et al., 2007; Mock et al., 2016); however, their vestibular function was normal (Jones et al., 2006). Future studies will be directed toward GAD2 progenitor-like cells in other strains and species. Although immunohistochemical experiments of intact whole-mount vertical cristae reveal an *EC* plexus, its origin, cellular composition, and function remain unknown.

Resource Availability

Lead Contact

Holly Holman (holly.holman@utah.edu).

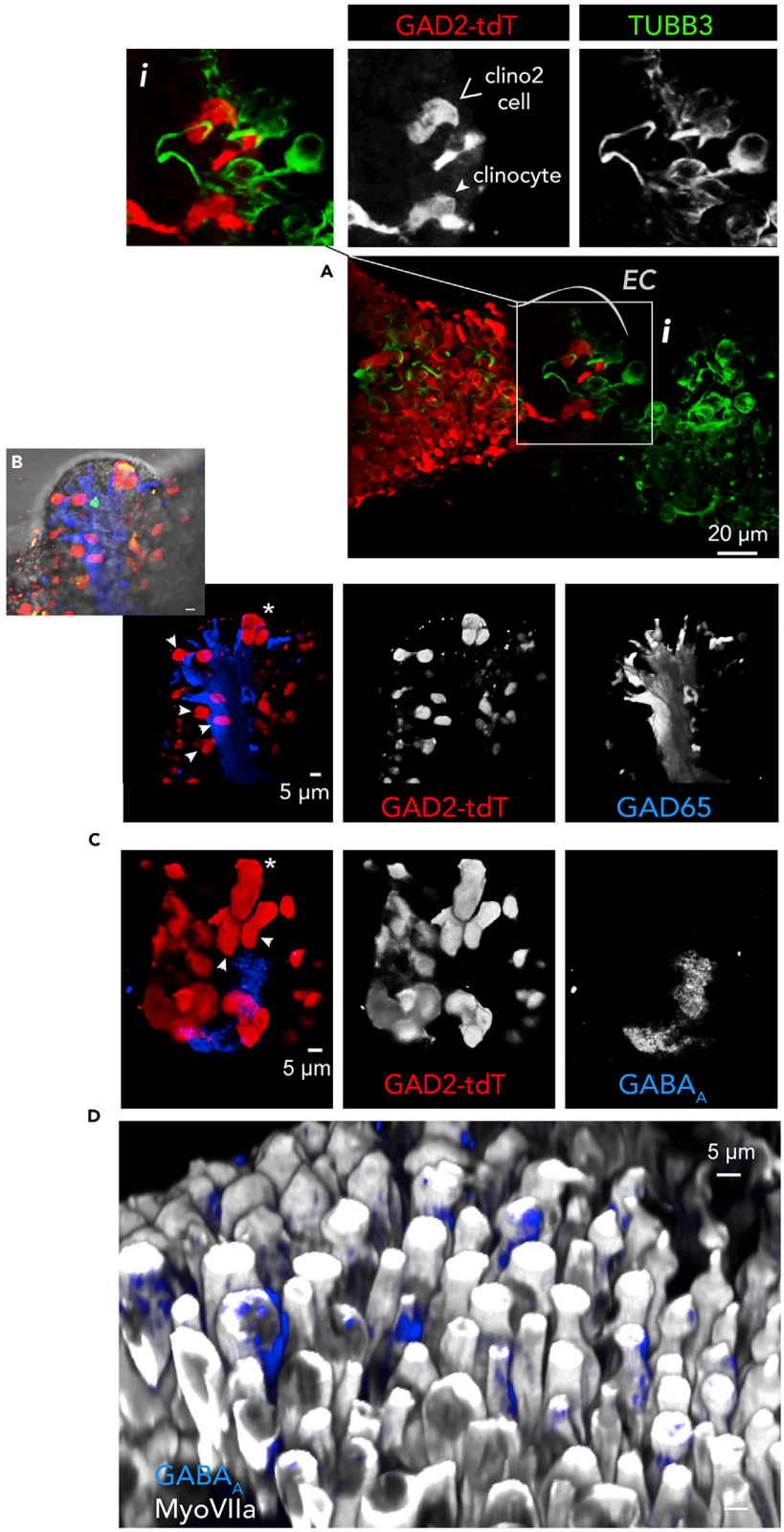
GAD2-tdT
TUBB3
i
clino2 cell
clinocyte
A
EC
i
20 μm
B
C
5 μm
GAD2-tdT
GAD65
5 μm
GAD2-tdT
GABA$_A$
D
5 μm
GABA$_A$
MyoVIIa

Figure 10. *EC* Plexus

(A) In a posterior canal crista from a mature mouse (P318, k = 1), βIII tubulin calyces (green) surround putative GAD2-tdT HCs (red). Few non-calyceal βIII tubulin fibers are observed near the *EC* with GAD2-tdT cells (red; box and inset, *i*).

(B) Anti-GAD65 antibody (blue) immunolabels the *EC* plexus in a mature mouse (P602, k = 1), where branches from the *EC* plexus contact a clino2 cell (*) and clinocytes (arrows).

(C) $GABA_A$ R immunolabeling (blue) within the *EC* near clino2 cell (star) and clinocytes (arrowheads) in a mature mouse (>2 years old, k = 1).

(D) $GABA_A$ R puncta near HCs (white; MyoVIIa) in a developing mouse crista (P6; k = 2; also see Video S8).

Materials Availability

This study did not generate new unique materials.

Data and Code Availability

The published article includes all data generated or analyzed during this study.

Data analysis software FluoRender and code are available on Github.

METHODS

All methods can be found in the accompanying Transparent Methods supplemental file.

SUPPLEMENTAL INFORMATION

Supplemental Information can be found online at https://doi.org/10.1016/j.isci.2020.101407.

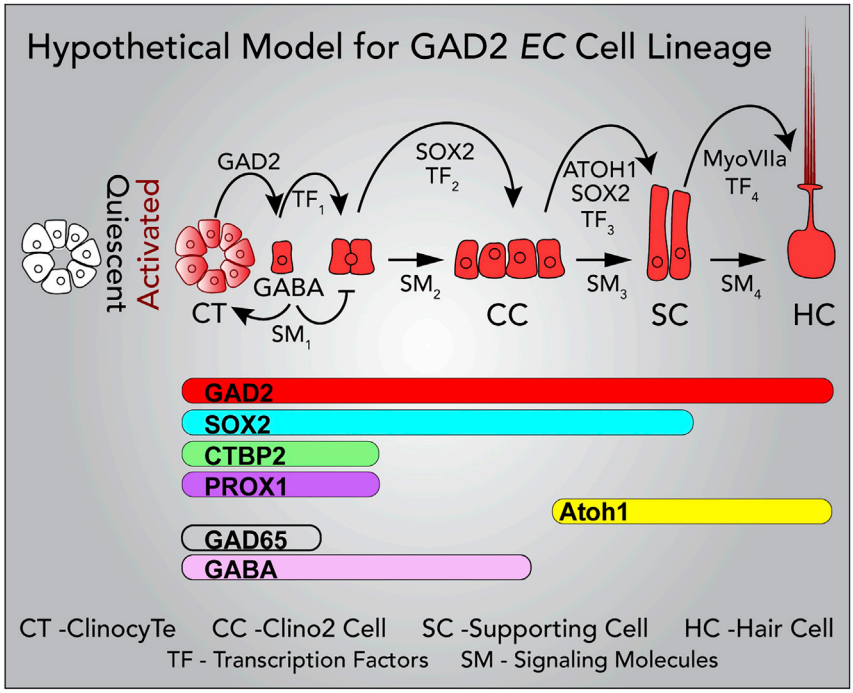

Figure 11. Hypothetical Model of Clinocyte and Clino2 Cell Lineage

A hypothetical model depicting GAD2 progenitor-like clinocyte cells (CTs) and their organization into rosettes, which are maintained in a quiescent state (far left). When GAD2 is transcribed in clinocytes and GAD65 is expressed these cells can synthesize GABA. Hypothetical release of GABA from CTs may provide a signaling mechanism that allowing a quiescent state and continuous rosette formation. Signaling molecules (SM_{1-4}) and transcriptional factors (TF_{1-4}), represent factors in the hypothetical clinocyte cell lineage. Regulation of GABA synthesis in CTscould maintain TFs and SMs keeping clinocytes in a quiescent state. Transient GABA could promote cell division of clinocytes into clino2 cells (CC; TF_2, SM_2). Transcriptional factors CTBP2, PROX1, and SOX2 in clinocytes may be actively involved at this stage. Differentiation of clino2 cells with key transcription factors (TF_3) and signaling molecules (SM_3) may lead to immature supporting cells (SC) that express ATOH1. A possible mechanism for generating GAD2 hair cells (HCs; MyoVIIa) with TF_4 and SM_4.

ACKNOWLEDGMENTS

This study was supported by a grant from the NIH: R01DC006685; P41 GM103545 and R01 EB023947 funded the development of the FluoRender analysis tool. The authors are grateful to Matthew Wachowiak, Karen Wilcox, Michael Deans, Larry Hoffman, Chris Holt, Richard Altschuler, and lab members for constructive suggestions and assistance with reagents. We thank Micah Frerck for the swept field confocal microscope build. We thank Colin Kitz for vestibular function testing. We thank Julia Peterson and Emma Lamae for illustrations.

AUTHOR CONTRIBUTIONS

Conceptualization, H.A.H.; Experiments, H.A.H.; Live-Cell Methodology, H.A.H. and R.D.R.; Cell Volume Analysis, H.A.H., Y.W., R.D.R.; Writing – Original Draft, H.A.H; Writing – Review & Editing, all authors.

DECLARATION OF INTERESTS

The authors report no competing interest.

Received: May 18, 2020
Revised: June 29, 2020
Accepted: July 21, 2020
Published: August 21, 2020

REFERENCES

Atkinson, P.J., Dong, Y., Gu, S., Gu, S., Liu, W., Najarro, E.H., Udagawa, T., and Cheng, A.G. (2018). SOX2 haploinsufficiency primes regeneration and Wnt responsiveness in the mouse cochlea. J. Clin. Invest. *128*, 1641–1656.

Baird, R.A., Desmadryl, G., Fernández, C., and Goldberg, J.M. (1988). The vestibular nerve of the chinchilla. II. Relation between afferent response properties and peripheral innervation patterns in the semicircular canals. J. Neurophysiol. *60*, 182–203.

Berekméri, E., Szepesy, J., Köles, L., and Zelles, T. (2019). Purinergic signaling in the organ of Corti: potential therapeutic targets of sensorineural hearing losses. Brain Res. Bull. *151*, 109–118.

Bermingham-McDonogh, O., and Rubel, E.W. (2003). Hair cell regeneration: winging our way towards a sound future. Curr. Opin. Neurobiol. *13*, 119–126.

Bootman, M.D., Collins, T.J., Mackenzie, L., Roderick, H.L., Berridge, M.J., and Peppiatt, C.M. (2002). 2-aminoethoxydiphenyl borate (2-APB). is a reliable blocker of store-operated Ca2+ entry but an inconsistent inhibitor of InsP3-induced Ca2+ release. FASEB J. *16*, 1145–1150.

Bowers, G., Cullinan, W.E., and Herman, J.P. (1998). Region-specific regulation of glutamic acid decarboxylase (GAD) mRNA expression in central stress circuits. J. Neurosci. *18*, 5938–5947.

Brignull, H.R., Raible, D.W., and Stone, J.S. (2009). Feathers and fins: non-mammalian models for hair cell regeneration. Brain Res. *1277*, 12–23.

Burns, J.C., and Stone, J.S. (2017). Development and regeneration of vestibular hair cells in mammals. Semin. Cell Dev. Biol. *65*, 96–105.

Catavero, C., Bao, H., and Song, J. (2018). Neural mechanisms underlying GABAergic regulation of adult hippocampal neurogenesis. Cell Tissue Res. *371*, 33–46.

Chagnaud, B.P., Engelmann, J., Fritzsch, B., Glover, J.C., and Straka, H. (2017). Sensing external and self-motion with hair cells: a comparison of the lateral line and vestibular systems from a developmental and evolutionary perspective. Brain Behav. Evol. *90*, 98–116.

Chen, C., Skellett, R.A., Fallon, M., and Bobbin, R.P. (1998). Additional pharmacological evidence that endogenous ATP modulates cochlear mechanics. Hear. Res. *118*, 47–61.

Cheng, C., Wang, Y., Guo, L., Lu, X., Zhu, W., Muhammad, W., Zhang, L., Lu, L., Gao, J., Tang, M., et al. (2019). Age-related transcriptome changes in SOX2+ supporting cells in the mouse cochlea. Stem Cell Res. Ther. *10*, 365.

Collazo, A., Bricaud, O., and Desai, K. (2005). Use of confocal microscopy in comparative studies of vertebrate morphology. Methods Enzymol. *395*, 521–543.

Corwin, J.T., and Cotanche, D.A. (1988). Regeneration of sensory hair cells after acoustic trauma. Science *240*, 1772–1774.

Coulter, D.A., and Carlson, G.C. (2007). Functional regulation of the dentate gyrus by GABA-mediated inhibition. Prog. Brain Res. *163*, 235–243.

Cruz, I.A., Kappedal, R., Mackenzie, S.M., Hailey, D.W., Hoffman, T.L., Schilling, T.F., and Raible, D.W. (2015). Robust regeneration of adult zebrafish lateral line hair cells reflects continued precursor pool maintenance. Dev. Biol. *402*, 229–238.

Dabdoub, A., Puligilla, C., Jones, J.M., Fritzsch, B., Cheah, K.S., Pevny, L.H., and Kelley, M.W. (2008). SOX2 signaling in prosensory domain specification and subsequent hair cell differentiation in the developing cochlea. Proc. Natl. Acad. Sci. U S A *105*, 18396–18401.

Desai, S.S., Ali, H., and Lysakowski, A. (2005a). Comparative morphology of rodent vestibular periphery. II. Cristae ampullaris. J. Neurophysiol. *93*, 267–280.

Desai, S.S., Zeh, C., and Lysakowski, A. (2005b). Comparative morphology of rodent vestibular periphery. I. Saccular and utricular maculae. J. Neurophysiol. *93*, 251–266.

Ding, J., Xu, H., Faiola, F., Ma'ayan, A., and Wang, J. (2012). Oct4 links multiple epigenetic pathways to the pluripotency network. Cell Res. *22*, 155–167.

Driver, E.C., Sillers, L., Coate, T.M., Rose, M.F., and Kelley, M.W. (2013). The Atoh1-lineage gives rise to hair cells and supporting cells within the mammalian cochlea. Dev. Biol. *376*, 86–98.

Dvorakova, M., Macova, I., Bohuslavova, R., Anderova, M., Fritzsch, B., and Pavlinkova, G. (2020). Early ear neuronal development, but not olfactory or lens development, can proceed without SOX2. Dev. Biol. *457*, 43–56.

Elkabetz, Y., and Studer, L. (2008). Human ESC-derived neural rosettes and neural stem cell progression. Cold Spring Harb. Symp. Quant. Biol. *73*, 377–387.

Esclapez, M., Tillakaratne, N.J., Kaufman, D.L., Tobin, A.J., and Houser, C.R. (1994). Comparative localization of two forms of glutamic acid decarboxylase and their mRNAs in rat brain supports the concept of functional differences between the forms. J. Neurosci. *14*, 1834–1855.

Fernández, C., Baird, R.A., and Goldberg, J.M. (1988). The vestibular nerve of the chinchilla. I. Peripheral innervation patterns in the horizontal and superior semicircular canals. J. Neurophysiol. *60*, 167–181.

Fernández, C., Lysakowski, A., and Goldberg, J.M. (1995). Hair-cell counts and afferent innervation patterns in the cristae ampullares of

the squirrel monkey with a comparison to the chinchilla. J. Neurophysiol. *73*, 1253–1269.

Forge, A., Li, L., Corwin, J.T., and Nevill, G. (1993). Ultrastructural evidence for hair cell regeneration in the mammalian inner ear. Science *259*, 1616–1619.

Fritzsch, B., Beisel, K.W., Jones, K., Fariñas, I., Lee, J., and Reichardt, L.F. (2002). Development and evolution of inner ear sensory epithelia and their innervation. J. Neurobiol. *53*, 143–156.

Fritzsch, B., Matei, V.A., Nichols, D.H., Bermingham, N., Jones, K., Beisel, K.W., and Wang, V.Y. (2005). Atoh1 null mice show directed afferent fiber growth to undifferentiated ear sensory epithelia followed by incomplete fiber retention. Dev. Dyn. *233*, 570–583.

Fritzsch, B., Eberl, D.F., and Beisel, K.W. (2010). The role of bHLH genes in ear development and evolution: revisiting a 10-year-old hypothesis. Cell. Mol. Life Sci. *67*, 3089–3099.

Fuentealba, L.C., Obernier, K., and Alvarez-Buylla, A. (2012). Adult neural stem cells bridge their niche. Cell Stem Cell *10*, 698–708.

Gee, M.J., Smith, N.A., Fernandez, F.R., Economo, M.N., Brunert, D., Rothermel, M., Morris, S.C., Talbot, A., Palumboset, S., Ichida, J.M., et al. (2014). Imaging activity in neurons and glia with a Polr2a-based and cre-dependent GCaMP5G-IRES-tdTomato reporter mouse. Neuron *83*, 1058–1072.

Giachino, C., Barz, M., Tchorz, J.S., Tome, M., Gassmann, M., Bischofberger, J., Bettler, B., and Taylor, V. (2014a). GABA suppresses neurogenesis in the adult hippocampus through GABAB receptors. Development *141*, 83–90.

Giachino, C., Basak, O., Lugert, S., Knuckles, P., Obernier, K., Fiorelli, R., Frank, S., Raineteau, O., Alvarez-Buylla, A., and Taylor, V. (2014b). Molecular diversity subdivides the adult forebrain neural stem cell population. Stem Cells *32*, 70–84.

Glowatzki, E., Ruppersberg, J.P., Zenner, H.P., and Rüsch, A. (1997). Mechanically and ATP-induced currents of mouse outer hair cells are independent and differentially blocked by d-tubocurarine. Neuropharmacology *36*, 1269–1275.

Goldberg, J.S., and Hirschi, K.K. (2009). Diverse roles of the vasculature within the neural stem cell niche. Regen. Med. *4*, 879–897.

Grando, S.A. (1997). Biological functions of keratinocyte cholinergic receptors. J. Investig. Dermatol. Symp. Proc. *2*, 41–48.

Gu, R., Brown, R.M., Hsu, C.-W., Cai, T., Crowder, A.L., Piazza, V.G., Vadakkan, T.J., Dickinson, M.E., and Groves, A.K. (2016). Lineage tracing of SOX2-expressing progenitor cells in the mouse inner ear reveals a broad contribution to non-sensory tissues and insights into the origin of *Corti*. Dev. Biol. *414*, 72–84.

Harada, Y. (1972). Observations of the crista ampullaris with the scanning electron microscopy. Nihon Jibiinkoka Gakkai Kaiho *75*, 546–549.

Harada, Y. (1983). Atlas of the Ear: By Scanning Electron Microscopy (MTP Press Limited).

Harding, M.J., McGraw, H.F., and Nechiporuk, A. (2014). The roles and regulation of multicellular rosette structures during morphogenesis. Development *141*, 2549–2558.

Holman, H.A., Poppi, L.A., Frerck, M., and Rabbitt, R.D. (2019). Spontaneous and acetylcholine evoked calcium transients in the developing mouse utricle. Front. Cell. Neurosci. *13*, 186.

Holt, J.C., Jordan, P.M., Lysakowski, A., Shah, A., Barsz, K., and Contini, D. (2017). Muscarinic acetylcholine receptors and M-currents underlie efferent-mediated slow excitation in calyx-bearing vestibular afferents. J. Neurosci. *37*, 1873–1887.

Houser, C.R. (2007). Interneurons of the dentate gyrus: an overview of cell types, terminal fields and neurochemical identity. Prog. Brain Res. *163*, 217–232.

Housley, G.D., Luo, L., and Ryan, A.F. (1998). Localization of mRNA encoding the P2X2 receptor subunit of the adenosine 5′-triphosphate-gated ion channel in the adult and developing rat inner ear by in situ hybridization. J. Comp. Neurol. *393*, 403–414.

Housley, G.D., Kanjhan, R., Raybould, N.P., Greenwood, D., Salih, S.G., Järlebark, L., Burton, L.D., Setz, V.C., Cannell, M.B., Soeller, C., et al. (1999). Expression of the P2X(2) receptor subunit of the ATP-gated ion channel in the cochlea: implications for sound transduction and auditory neurotransmission. J. Neurosci. *19*, 8377–8388.

Igarashi, M., and Alford, B.R. (1969). Cupula, cupular zone of otolithic membrane, and tectorial membrane in the squirrel monkey. Acta Otolaryngol. *68*, 420–426.

Igarashi, M., and Yoshinobu, T. (1966). Comparative observations of the eminentia cruciata in birds and mammals. Anat. Rec. *155*, 269–277.

Ihrie, R.A., and Alvarez-Buylla, A. (2011). Lake-front property: a unique germinal niche by the lateral ventricles of the adult brain. Neuron *70*, 674–686.

Ison, J.R., Allen, P.D., and O'Neill, W.E. (2007). Age-related hearing loss in C57BL/6J mice has both frequency-specific and non-frequency-specific components that produce a hyperacusis-like exaggeration of the acoustic startle reflex. J. Assoc. Res. Otolaryngol. *8*, 539–550.

Järlebark, L.E., Housley, G.D., and Thorne, P.R. (2000). Immunohistochemical localization of adenosine 5′-triphosphate-gated ion channel P2X(2) receptor subunits in adult and developing rat cochlea. J. Comp. Neurol. *421*, 289–301.

Järlebark, L.E., Housley, G.D., Raybould, N.P., Vlajkovic, S., and Thorne, P.R. (2002). ATP-gated ion channels assembled from P2X2 receptor subunits in the mouse cochlea. Neuroreport *13*, 1979–1984.

Jiang, L., Romero-Carvajal, A., Haug, J.S., Seidel, C.W., and Piotrowski, T. (2014). Gene-expression analysis of hair cell regeneration in the zebrafish lateral line. Proc. Natl. Acad. Sci. U S A *111*, E1383–E1392.

Jin, K., Minami, M., Lan, J.Q., Lan, J.Q., Mao, X.O., Batteur, S., Simon, R.P., and Greenberg, D.A. (2001). Neurogenesis in dentate subgranular zone and rostral subventricular zone after focal cerebral ischemia in the rat. Proc. Natl. Acad. Sci. U S A *98*, 4710–4715.

Jones, S.M., Jones, T.A., Johnson, K.R., Yu, H., Erway, L.C., and Zheng, Q.Y. (2006). A comparison of vestibular and auditory phenotypes in inbred mouse strains. Brain Res. *1091*, 40–46.

Kanaani, J., Lissin, D., Kash, S.F., and Baekkeskov, S. (1999). The hydrophilic isoform of glutamate decarboxylase, GAD67, is targeted to membranes and nerve terminals independent of dimerization with the hydrophobic membrane-anchored isoform, GAD65. J. Biol. Chem. *274*, 37200–37209.

Kass, I., Hoke, D.E., Costa, M.G., Reboul, C.F., Porebski, B.T., Cowieson, N.P., Leh, H., Pennacchietti, E., McCoey, J., Kleifelet, O., et al. (2014). Cofactor-dependent conformational heterogeneity of GAD65 and its role in autoimmunity and neurotransmitter homeostasis. Proc. Natl. Acad. Sci. U S A *111*, E2524–E2529.

Kempfle, J.S., Turban, J.L., and Edge, A.S. (2016). SOX2 in the differentiation of cochlear progenitor cells. Sci. Rep. *6*, 23293.

Kiernan, A.E., Pelling, A.L., Leung, K.K., Tang, A.S.P., Bell, D.M., Tease, C., Lovell-Badge, R., Steel, K.P., and Cheah, K.S.E. (2005). SOX2 is required for sensory organ development in the mammalian inner ear. Nature *434*, 1031–1035.

Kim, J.Y., Liu, C.Y., Zhang, F., Duan, X., Wen, Z., Song, J., Feighery, E., Lu, B., Rujescu, D., Clair, D.S., et al. (2012). Interplay between DISC1 and GABA signaling regulates neurogenesis in mice and risk for schizophrenia. Cell *148*, 1051–1064.

Kim, T.W., Kang, B.H., Jang, H., Kwak, S., Shin, J., Kim, H., Lee, S.-E., Lee, S.-M., Lee, J.-H., Kim, J.-H., et al. (2015). CTBP2 modulates NuRD-mediated deacetylation of H3K27 and facilitates PRC2-mediated H3K27me3 in active embryonic stem cell genes during exit from pluripotency. Stem Cells *33*, 2442–2455.

Kirjavainen, A., Sulg, M., Heyd, F., Alitalo, K., Ylä-Herttuala, S., Möröy, T., Petrova, T.V., and Pirvola, U. (2008). PROX1 interacts with Atoh1 and Gfi1, and regulates cellular differentiation in the inner ear sensory epithelia. Dev. Biol. *322*, 33–45.

Kniss, J.S., Jiang, L., and Piotrowski, T. (2016). Insights into sensory hair cell regeneration from the zebrafish lateral line. Curr. Opin. Genet. Dev. *40*, 32–40.

Kujawa, S.G., and Liberman, M.C. (2009). Adding insult to injury: cochlear nerve degeneration after "temporary" noise-induced hearing loss. J. Neurosci. *29*, 14077–14085.

Landgraf, D., Barth, M., Layer, P.G., and Sperling, L.E. (2010). Acetylcholine as a possible signaling molecule in embryonic stem cells: studies on survival, proliferation and death. Chem. Biol. Interact. *187*, 115–119.

Lewis, E.R., Leverenz, E.L., and Bialek, W.S. (1985). The Vertebrate Inner Ear (CRC-Press).

Lim, D.J. (1976). Morphological and physiological correlates in cochlear and vestibular sensory epithelia. In Scanning Electron Microscopy/1976/

II (Illinois Institute of Technology Research Institute), pp. 269–276.

Lindeman, H.H. (1969). Studies on the morphology of the sensory regions of the vestibular apparatus with 45 figures. Ergeb Anat. Entwicklungsgesch *42*, 1–113.

Liu, S., Wang, Y., Lu, Y., Li, W., Liu, W., Ma, J., Sun, F., Li, M., Chen, Z.-Y., Su, K., and Li, W. (2018). The key transcription factor expression in the developing vestibular and auditory sensory organs: a comprehensive comparison of spatial and temporal patterns. Neural Plast. *2018*, 7513258.

Locher, H., Frijns, J.H.M., van Iperen, L., de Groot, J.C.M., Huisman, M.A., Chuva, S.M., and Lopes, deS. (2013). Neurosensory development and cell fate determination in the human cochlea. Neural Dev. *8*, 20.

Lush, M.E., and Piotrowski, T. (2014). Sensory hair cell regeneration in the zebrafish lateral line. Dev. Dyn. *243*, 1187–1202.

Lush, M.E., Diaz, D.C., Koenecke, N., Baek, S., Boldt, H., Peter, M.S., Gaitan-Escudero, T., Romero-Carvajal, A., Busch-Nentwich, E.M., and Perera, A.G. (2019). scRNA-Seq reveals distinct stem cell populations that drive hair cell regeneration after loss of Fgf and Notch signaling. Elife *8*, e44431.

Lysakowski, A. (1996). Synaptic organization of the crista ampullaris in vertebrates. Ann. N. Y. Acad. Sci. *781*, 164–182.

Lysakowski, A., and Goldberg, J.M. (1997). A regional ultrastructural analysis of the cellular and synaptic architecture in the chinchilla cristae ampullares. J. Comp. Neurol. *389*, 419–443.

McLean, W.J., Yin, X., Lu, L., Lenz, D.R., McLean, D., Langer, R., Karp, J.M., and Edge, A.S.B. (2017). Clonal expansion of Lgr5-positive cells from mammalian cochlea and high-purity generation of sensory hair cells. Cell Rep. *18*, 1917–1929.

Merkle, F.T., Mirzadeh, Z., and Alvarez-Buylla, A. (2007). Mosaic organization of neural stem cells in the adult brain. Science *317*, 381–384.

Mirzadeh, Z., Merkle, F.T., Soriano-Navarro, M., Garcia-Verdugo, J.M., and Alvarez-Buylla, A. (2008). Neural stem cells confer unique pinwheel architecture to the ventricular surface in neurogenic regions of the adult brain. Cell Stem Cell *3*, 265–278.

Mock, B.E., Vijayakumar, S., Pierce, J., Jones, T.A., and Jones, S.M. (2016). Differential effects of Cdh23(753A) on auditory and vestibular functional aging in C57BL/6J mice. Neurobiol. Aging *43*, 13–22.

Neves, J., Vachkov, I., and Giraldez, F. (2013). SOX2 regulation of hair cell development: incoherence makes sense. Hear. Res. *297*, 20–29.

Paraoanu, L.E., Boutter, J., Landgraf, D., Barth, M., Wessler, and Layer, P. (2007a). Cholinesterases and cholinergic system in embryonic stem cell regulation: data on gene expression and functions. J. Stem Cells Regen. Med. *2*, 139.

Paraoanu, L.E., Steinert, G., Koehler, A., Wessler, I., and Layer, P.G. (2007b). Expression and possible functions of the cholinergic system in a murine embryonic stem cell line. Life Sci. *80*, 2375–2379.

Parker, M.S., Larroque, M.L., Campbell, J.M., Bobbin, R.P., and Deininger, P.L. (1998). Novel variant of the P2X2 ATP receptor from the Guinea pig organ of Corti. Hear. Res. *121*, 62–70.

Puligilla, C., and Kelley, M.W. (2017). Dual role for SOX2 in specification of sensory competence and regulation of Atoh1 function. Dev. Neurobiol. *77*, 3–13.

Rossi, M.L., Prigioni, I., Gioglio, L., Rubbini, G., Russo, G., Martini, M., Farinelli, F., Rispoli, G., and Fesce, R. (2006). IP3 receptor in the hair cells of frog semicircular canal and its possible functional role. Eur. J. Neurosci. *23*, 1775–1783.

Ryals, B.M., and Rubel, E.W. (1988). Hair cell regeneration after acoustic trauma in adult Coturnix quail. Science *240*, 1774–1776.

Salih, S.G., Housley, G.D., Raybould, N.P., and Thorne, P.R. (1999). ATP-gated ion channel expression in primary auditory neurones. Neuroreport *10*, 2579–2586.

Scheffer, D.I., Shen, J., Corey, D.P., and Chen, Z.Y. (2015). Gene expression by mouse inner ear hair cells during development. J. Neurosci. *35*, 6366–6380.

Sergeyenko, Y., Lall, K., Liberman, M.C., and Kujawa, S.G. (2013). Age-related cochlear synaptopathy: an early-onset contributor to auditory functional decline. J. Neurosci. *33*, 13686–13694.

Serobyan, N., Jagannathan, S., Orlovskaya, I., Schraufstatter, I., Skok, M., Loring, J., and Khaldoyanidi, S. (2007). The cholinergic system is involved in regulation of the development of the hematopoietic system. Life Sci. *80*, 2352–2360.

Shook, B.A., Manz, D.H., Peters, J.J., Kang, S., and Conover, J.C. (2012). Spatiotemporal changes to the subventricular zone stem cell pool through aging. J. Neurosci. *32*, 6947–6956.

Slowik, A.D., and Bermingham-McDonogh, O. (2016). A central to peripheral progression of cell cycle exit and hair cell differentiation in the developing mouse cristae. Dev. Biol. *411*, 1–14.

Steevens, A.R., Glatzer, J.C., Kellogg, C.C., Low, W.C., Santi, P.A., and Kiernan, A.E. (2019). SOX2 is required for inner ear growth and cochlear nonsensory formation before sensory development. Development *146*, dev170522.

Sueta, T., Paki, B., Everett, A.W., and Robertson, D. (2003). Purinergic receptors in auditory neurotransmission. Hear. Res. *183*, 97–108.

Suh, M.Y., Kim, T.W., Lee, H.-T., Shin, J., Kim, J.-H., Jang, H., Kim, H.J., Kim, S.-T., Cho, E.-J., and Youn, H.-D. (2018). Abundance of C-terminal binding protein isoform is a prerequisite for exit from pluripotency in mouse embryonic stem cells. FASEB J. *32*, 6423–6435.

Szücs, A., Szappanos, H., Tóth, A., Farkas, Z., Panyi, G., Csernoch, L., and Sziklai, I. (2004). Differential expression of purinergic receptor subtypes in the outer hair cells of the Guinea pig. Hear. Res. *196*, 2–7.

Taheri, M., Handy, G., Borisyuk, A., and White, J.A. (2017). Diversity of evoked astrocyte Ca^{2+} dynamics quantified through experimental measurements and mathematical modeling. Front. Syst. Neurosci. *11*, 79.

Takahashi, T., Ohnishi, H., Sugiura, Y., Honda, K., Suematsu, M., Kawasaki, T., Deguchi, T., Fujii, T., Orihashi, K., Hippo, Y., et al. (2014). Non-neuronal acetylcholine as an endogenous regulator of proliferation and differentiation of Lgr5-positive stem cells in mice. FEBS J. *281*, 4672–4690.

Taniguchi, H., He, M., Wu, P., Kim, S., Paik, R., Sugino, K., Kvitsiani, D., Fu, Y., Lu, J., Lin, Y., et al. (2011). A resource of Cre driver lines for genetic targeting of GABAergic neurons in cerebral cortex. Neuron *71*, 995–1013.

Tapia, N., MacCarthy, C., Esch, D., Marthaler, A.G., Tiemann, U., Araúzo-Bravo, M.J., Jauch, R., Cojocaru, V., and Schöler, H.R. (2015). Dissecting the role of distinct OCT4-SOX2 heterodimer configurations in pluripotency. Sci. Rep. *5*, 13533.

Tarleton, H.P., and Lemischka, I.R. (2010). Delayed differentiation in embryonic stem cells and mesodermal progenitors in the absence of CTBP2. Mech. Dev. *127*, 107–119.

Tavazzani, E., Tritto, S., Spaiardi, P., Botta, L., Manca, M., Prigioni, I., Masetto, S., and Russo, G. (2014). Glutamic acid decarboxylase 67 expression by a distinct population of mouse vestibular supporting cells. Front. Cell. Neurosci. *8*, 428.

Telang, R.S., Paramananthasivam, V., Vlajkovic, S.M., Munoz, D.J., Housley, G.D., and Thorne, P.R. (2010). Reduced P2x(2) receptor-mediated regulation of endocochlear potential in the ageing mouse cochlea. Purinergic Signal. *6*, 263–272.

Tochitani, S., and Kondo, S. (2013). Immunoreactivity for GABA, GAD65, GAD67 and Bestrophin-1 in the meninges and the choroid plexus: implications for non-neuronal sources for GABA in the developing mouse brain. PLoS One *8*, e56901.

Tozuka, Y., Fukuda, S., Namba, T., Seki, T., and Hisatsune, T. (2005). GABAergic excitation promotes neuronal differentiation in adult hippocampal progenitor cells. Neuron *47*, 803–815.

van den Berg, D.L., Snoek, T., Mullin, N.P., Yates, A., Bezstarosti, K., Demmers, J., Chambers, I., and Poot, R.A. (2010). An Oct4-centered protein interaction network in embryonic stem cells. Cell Stem Cell *6*, 369–381.

Wan, L., Lovett, M., Warchol, M.E., and Stone, J.S. (2020). Vascular endothelial growth factor is required for regeneration of auditory hair cells in the avian inner ear. Hear. Res. *385*, 107839.

Wang, J.C., Raybould, N.P., Luo, L., Ryan, A.F., Cannell, M.B., Thorne, P.R., and Housley, G.D. (2003). Noise induces up-regulation of P2X2 receptor subunit of ATP-gated ion channels in the rat cochlea. Neuroreport *14*, 817–823.

Warchol, M.E., Lambert, P.R., Goldstein, B.J., Forge, A., and Corwin, J.T. (1993). Regenerative proliferation in inner ear sensory epithelia from adult Guinea pigs and humans. Science *259*, 1619–1622.

Wessler, I., and Kirkpatrick, C.J. (2008). Acetylcholine beyond neurons: the non-neuronal

cholinergic system in humans. Br. J. Pharmacol. *154*, 1558–1571.

Wessler, I., Kirkpatrick, C.J., and Racké, K. (1998). Non-neuronal acetylcholine, a locally acting molecule, widely distributed in biological systems: expression and function in humans. Pharmacol. Ther. *77*, 59–79.

Wilkerson, B.A., Chitsazan, A.D., VandenBosch, L.S., Wilken, M.S., Reh, T.A., and Bermingham-McDonogh, O. (2019). Open chromatin dynamics in prosensory cells of the embryonic mouse cochlea. Sci. Rep. *9*, 9060.

Williams, B.P., Milligan, C.J., Street, M., Hornby, F.M., Deuchars, J., and Buckley, N.J. (2004). Transcription of the M1 muscarinic receptor gene in neurons and neuronal progenitors of the embryonic rat forebrain. J. Neurochem. *88*, 70–77.

Yan, L.F., and Gu, A.H. (2013). Progress and application of zebrafish in regenerative medicine. Yi Chuan *35*, 856–866.

Yang, L.M., Cheah, K.S.E., Huh, S.H., and Ornitz, D.M. (2019). SOX2 and FGF20 interact to regulate organ of Corti hair cell and supporting cell development in a spatially-graded manner. PLoS Genet. *15*, e1008254.

Zhao, H.B., Yu, N., and Fleming, C.R. (2005). Gap junctional hemichannel-mediated ATP release and hearing controls in the inner ear. Proc. Natl. Acad. Sci. U S A *102*, 18724–18729.

iScience, Volume *23*

Supplemental Information

Developmental GAD2 Expression Reveals Progenitor-like Cells with Calcium Waves in Mammalian Crista Ampullaris

Holly A. Holman, Yong Wan, and Richard D. Rabbitt

Supplemental Information

Transparent Methods

Mouse Strains and Transgenic Lines

All animal experiments were approved by the University of Utah Institutional Animal Care and Use Committee in accordance with NIH guidelines and conducted at the University of Utah. In this study, the wild-type parental strain C57BL/6J and three transgenic mouse lines were utilized: a dual Cre-dependent reporter Polr2a-based GCaMP5G-IRES-tdTomato, referred to as PC::G5-tdT (Gee et al., 2014) and a GAD2-IRES-Cre knock-in mouse driver line referred to as GAD2::Cre (Taniguchi et al., 2011). Both transgenic breeding pairs were obtained from The Jackson Laboratory (Polr2a$^{tm1(CAG-GCaMP5g,-tdTomato)Tvrd}$ jax.org/strain/024477; GAD2$^{tm2(cre)Zjh}$ jax.org/strain/010802). First generation heterozygous offspring were used in all experiments and referred to as GAD2-tdT and GAD2-G5::tdT. Parental wild-type (WT) control mice (C57BL/6J jax.org/strain/0000664) were used in age-matched experiments. The Tg(Atoh1-cre)1Bfri line was crossed with the dual Cre-dependent reporter Polr2a-based GCaMP5G-IRES-tdTomato to control for GAD2-Cre transgenic expression (B6.Cg-Tg(Atoh1-cre)1Bfri/J; jax.org/strain/011104). Offspring were genotyped using real-time PCR (probes: 'Polr2a-3', 'GCamp3-1 Tg' and 'tdRFP'; (Transnetyx, Inc.)). The parental strain C57BL/6J carries a cadherin 23 mutation leading to early onset hearing loss, but aging of the vestibular system is minimal in these mice with no evidence of early onset vestibular dysfunction (Mock et al., 2016**).** Although inbred A/J mice can exhibit early onset vestibular deficits (Vijayakumar et al., 2016), a sampling of adult transgenic mice used in this study demonstrated normal vestibular functions by qualitative balance beam and rotarod testing (Colin Kitz, unpublished data).

Fixed Tissue Processing and Image Analysis

Seventy-eight mice from both sexes provided immunohistology data with the following numbers in each age group: P0-7 (k=33), P8-55 (k=22), P170-P365 (k=9), P366-P936 (k=9). For immunohistochemistry preparations, intact membranous labyrinths were harvested, and immersion fixed in 4% paraformaldehyde overnight at 4°C. Whole mount neuroepithelia were exposed by micro-dissections, using fine forceps in 0.1M phosphate-buffered saline (PBS) (Dumont #5, #55; Leica, M165 FC).

Whole Mount Immunohistochemistry

Membranous labyrinths were incubated transiently three times in 0.1M PBS to remove residual aldehydes, followed by incubation in a blocking/permeabilization buffer (10% normal serum specific to the antisera (*i.e.* goat), 1% BSA, 0.5% Triton X-100 in 0.1M PBS) for 1-2 hr on a rocker platform at room temperature (RT). Tissues were subsequently incubated overnight at 4°C with one of or a combination of the following primary antisera: anti-Atoh1 (SAB2100177, Sigma); anti-ChAT (choactase (E-7) AlexaFluor® 488, Santa Cruz); anti-VAChT (SAB4200559, Millipore); anti-VGAT (131002; Synaptic Systems); anti-CTBP2 (612044, BD Transduction); anti-mAChR M1:G-9) (sc-365966, Santa Cruz); mAChR M2:M2-2-B3) (sc-33712, Santa Cruz); anti-GAD65 (MAB351; Sigma); anti-GAD67 (PA5-21397; ThermoFisher Scientific); anti-SOX2 (sc-365823, Santa Cruz); and anti-MyosinVIIa (25-6790, Proteus Biosciences); anti-PROX1 (PA5-85552, Invitrogen); and monoclonal mouse anti-Tubulin β3 antibody conjugated with AlexaFluor® 647 (801209, BioLegend). Primary antibodies were used with dilutions ranging from 1:50 to 1:500 in blocking/permeabilization buffer. Tissues were subsequently rinsed three times for 15 min in 0.1M PBS, then placed in fresh blocking buffer and incubated for another 1 h at RT with secondary antisera conjugated to either AlexaFluor® (donkey anti-rabbit IgG H&L 405nm (ab175651), DyLight™ 405nm (35550), or 488nm (35552), Thermo Scientific,

Inc.). After incubations with secondary antisera, tissues were gently rinsed three times in PBS, placed onto glass bottom dishes (MatTek) with 0.1M PBS for confocal imaging (Olympus, FV1000). Z-stacks were acquired using either 5X air (N.A. 0.1) to orient whole mount tissues, or higher resolution 40X water (N.A. 0.8), or 60X water (N.A. 1.0) objectives for cellular structures with digital zoom up to 3X, and aspect ratio of 620 x 620 pixels.

GAD2 Cell Volume FluoRender Analysis

FluoRender was used to perform a detailed analysis on cell volume from confocal z-stack image datasets. In the tdTomato 3D confocal channel, cells were segmented, individually inspected, and classified based on morphology. Then, cell sizes in each category were statistical analyzed. FluoRender (v2.24.2) was downloaded from Github (https://github.com/SCIInstitute/fluorender/releases).

For each age group, we examined all confocal scans three-dimensionally and selected one with the best clarity for analysis. We loaded the selected confocal scan, in the Olympus Image Binary (OIB) format, into FluoRender. A typical scan consisted of four channels (3 fluorescent channels plus a phase contrast channel). The segmentation and classification of cells were only performed on the tdTomato channel. Therefore, we isolated the display to only the tdTomato channel in FluoRender. To generate an initial unrefined segmentation on the cells, we used the Component Analyzer function in FluoRender. Because the cells were expected to be smaller than 30 voxels in length, we set the Iteration of the Component Analyzer to 30. Then, we estimated and set the threshold value to 0.45 for separating the cells. After generating the initial segmentation, individual cells were labelled with unique IDs and associated colors. Since scans from various age groups differed in intensity distributions, the settings to generate the initial segmentation varied. To fine-tune the threshold setting for each scan, we enabled the Auto Update function in FluoRender's Component Analyzer. This allowed segmentation

results to be updated interactively when the threshold setting was changed. For the initial segmentation, we paid attention to the most easily discernable cellular structures and adjusted the threshold value to correctly separate from background and from each other. Furthermore, a refined segmentation was obtained using FluoRender's freehand selection functions. In the Component Analyzer, we enabled a feature called Use Selection, which restricted the segmentation to masked regions from freehand selections, while preserving the existing results outside of the masks. This method efficiently segments cells of low intensity signals excluded by the initial threshold. To enhance the intensity signals for easy freehand selections, we lowered both the Saturation and Gamma values of the scan. Then, we enabled the Select brush tool in FluoRender and painted on the low intensity cells to generate a mask that only included them. To segment the selected low intensity cells, we lowered the threshold value of the Component Analyzer and generated components. The resulting colors of the selected cells were closely observed to ensure accurate segmentations. Again, the Auto Update function was enabled to obtain an appropriate threshold value for each selected cell. We found that, for the majority of low-intensity cells, a decrease of around 0.1 to the threshold value would be sufficient; certain cells of very low intensity values required the threshold value to be lowered by around 0.2. The segmented cells were pruned according to their voxel counts. We excluded any segmented structures smaller than 100 voxels. Larger structures outside of the area of interest were manually pruned. We examined the remaining cells three-dimensionally and evaluated their morphology. Cells were individually selected and grouped accordingly. For each cell group, we generated a selection mask and saved the results in FluoRender's project file. Then, we computed a list comprising the physical size of each cell for each cell group. A cell's physical size was computed as the product of its voxel count and the physical size of a single voxel (in μm^3), which was part of the information retrieved from the confocal metadata.

For clear visualization of clino2 cells and clinocytes, three-dimensional models were reconstructed from isolated volume data. We first used FluoRender to convert segmented cells into mesh files. The mesh files were loaded into Autodesk Maya (v2017, Autodesk, Inc.) for clearing and smoothing. We assigned material in Maya to give the cell models an organic appearance.

Live Cell Imaging and Analysis

Thirty-six mice provided physiological data with the following numbers in each age group: P1 (k=6), P2-3 (k=5), P5-8 (k=5), P9-11 (k=6), P14-18 (k=6), P21-53 (k=4), P108-825 (k=4). Mice were deeply anesthetized with ketamine (100 mg/kg body weight) and xylazine (10 mg/kg). GAD2::G5-tdT mice were decapitated and the bony labyrinth dissected in cold glycerol-modified Ringer's (in mM: 26 $NaHCO_3$, 11 glucose, 250 glycerol, 2.5 KCl, 1.2 NaH_2PO4, 1.2 $MgCl_2$ and 2.4 $CaCl_2$; pH 7.4; Rabbitt et al., 2016). The utricle, horizontal crista, anterior crista and posterior crista were dissected in a semi-intact preparation from the temporal bone and the membranous labyrinth was cut open to expose apical surfaces of all three sensory epithelia (Lim et al., 2011). Tissue was transferred to an imaging chamber (Warner Instruments; RC-22C) and continuously perfused with room temperature physiology buffer (5.8 KCl, 144 NaCl, 0.9 $MgCl_2$, 1.3 $CaCl_2$, 0.7 NaH_2PO_4, 5.6 glucose, 10 HEPES, 300 mOsm, pH 7.4) (Sadeghi et al., 2014). The recording chamber was placed on the stage of a swept field confocal microscope (Bruker; Prairie SFC) and images were acquired with a water immersion 60x objective (Olympus). Confocal images were collected using a 35 µm slit aperture in linear galvanometer mode, and a 512 x 512 detector (Photometrics, Rolera MGi Plus EMCCD) providing in-plane single pixel size of 0.27 x 0.27 µm. For GCaMP5G detection and tdTomato expression, 488 nm and 561nm lasers, respectively, were interleaved for excitation, and a four-line blocking filter (Semrock, R405/488/561/635-25) was used for

detection. For G5 fluorescence calcium imaging, excitation was limited to 488nm and the detection filter was replaced with a band pass filter (Semrock 525/50-25) to block any residual tdT emission. A pressure driven perfusion system configured with a micro-manifold (ALA Scientific Instruments, VC3-4PP, uflow-4) was used to continuously wash the epithelium with control media, 100μM ACh, 100-300μM muscarine, 50μM 2-APB, and/or 50μM atropine (ATR). The SFC (Bruker; Prairie Link), stage position (Scientifica), and perfusion system (ALA) were controlled and monitored at 10kHz by custom software (WaveMetrics, Igor) *via* AD hardware (Heka, ITC-18), IEEE-488 instrumentation interface (National Instruments, GPIB-USB; Sony/Tektronix, AFG-320) and serial interface.

G5 fluorescence modulation was monitored at each "z" focal depth using a time sequence of images collected before, during, and after the ACh puff. Unless otherwise noted, image sequences consisted of 1000-2000 frames collected at 10 frames.s^{-1} (100-200 s image sequence). ACh or muscarine was delivered as a 500 ms puff 10s after initiating the sequence.

Quantification and Statistical Analysis

Each image was smoothed in (x,y) space with a 3 pixel Gaussian filter (WaveMetrics, Igor). To minimize motion artifact, time-sequences were registered in space using manually selected control regions of interest (Thévenaz et al., 1998). G5 fluorescence modulation was determined pixel-by-pixel using $\Delta F/F_{min}$, where $\Delta F=F(t)-F_{min}$ and F_{min} was the minimum fluorescence intensity in the pixel over the entire time-sequence of images. Unless otherwise noted, Ca^{2+} modulation is reported in images and animations (movies) in RGB format with G5 F_{min} shown in the blue channel and $\Delta F/F_{min}$ shown in the green channel. Statistical significance of differences in the mean between groups was determined using Student's t-test with p=0.05, unless stated otherwise. All population data were presented as a mean ± standard errors of the means.

Supplemental Figures

Figure S1. ATP Evoked Ca^{2+} Transients in Cochlea and Crista, *Related to Figure 4*.

ATP (100μM) evokes Ca^{2+} transients in cells of Köllicker's organ and the organ of Corti, but not in the novel cell niche of cristae at P1 (k=2). A) Resting G5 fluorescence (F0, blue) merged with peak change in G5 fluorescence (ΔF/F0, green) showing no response to application of 100μM ATP at P1. B) Merged G5 image of the apical turn of the cochlea from the same P1 ear showing ATP evoked Ca^{2+} transients in inner border cells. C-D) $\Delta F/F_0$ traces from individual cells showing no response to ATP in the crista and evoked responses in the cochlea. D-E) The latency of evoked transients in cochlear border cells was ~40s from the onset of the ATP puff. (Also see: Movie S1. P1 ATP). Dotted line signifies the tunnel of Corti (TC). "Inner" relates to cells adjacent to and including Inner Hair Cells, whereas "Outer" relates to cells surrounding and including Outer Hair cells.

Figure S2. ACh Evoked Ca^{2+} Transients Blocked by Atropine, *Related to Figure 5.*

A-B) Resting G5 fluorescence (F_0, blue), and peak change in, green) in response to 100μM ACh in anterior canal cristae (P3). C) Change in G5 fluorescence ($\Delta F/F_0$) from 50 μM ATR block. D) Relative change ACh evoked Ca^{2+} transients and extent of ATR block is shown by merging (A-C). A,E-F) ROIs from multiple clinocytes (black traces); three ROIs in different regions of one clino2 cell (green traces): apical (1), central (2), and basal (3); and two ROIs from a second clino2 cell (blue traces): apical (1) and central (2). E) ACh evoked Ca^{2+} transients in the control condition with long-lasting bursts of Ca^{2+} in both clino2 cells. F) Same ROIs as panel E in the presence of 50μM 2-APB shown on a ~10x log scale.

Figure S3. ACh Evoked Ca^{2+} Transients in *EC* cells in Second Postnatal Week and Adult Mice, *Related to Figure 6*.

A-C) During the second week of postnatal development (P10) clino2 cells (c), and clinocytes (cts) have spontaneous and ACh evoked Ca^{2+} transients. A) Image of an anterior canal *EC* with resting G5 fluorescence (F_0, blue) and peak changes in spontaneous G5 fluorescence ($\Delta F/F_0$, green). B) Maximum changes in ACh evoked G5 fluorescence $\Delta F/F_0$. C) ACh evoked calcium transients in clino2 cells and clinocytes at P1. D) *EC* from an adult mouse anterior canal *EC* (P140) with resting G5 fluorescence (F_0, blue) and peak changes in spontaneous G5 fluorescence ($\Delta F/F_0$, green). E) ACh evoked $\Delta F/F_0$, in clino2 (c), clinocytes (cts), and hair cell (HC) calyces (h. calyces) at P140. F) ACh evoked Ca^{2+} transients in clino2 cells and clinocytes at P140.

Figure S4. GAD2-tdT cells in Horizontal Canal Cristae, *Related to Figure 6*.

A-C) Resting G5 fluorescence (F_0, blue), and peak change in G5 fluorescence ($\Delta F/F_0$, green) in response to 100μM ACh in horizontal canal cristae. The horizontal crista in mouse lacks a central *EC*, but resting G5 fluorescence, spontaneous and ACh evoked $\Delta F/F_0$ transients were observed with waveforms similar to those in the *EC* of anterior and posterior canal cristae. Results are consistent with the hypothesis that these cells are clinocytes. Highly expressing hair cells show strong G5 fluorescence at rest (blue) in somata and hair cell bundles (hcb). D) A small number of cells with strong G5 resting fluorescence in horizontal cristae responded with large $\Delta F/F_0$ transients consistent with clino in *EC* of anterior and posterior cristae. E) Other cells with resting G5 fluorescence responded to 100μM ACh with brief Ca^{2+} transients consistent with clinocytes in *EC* of anterior and posterior canal cristae. A subset of these hypothetical clinocytes exhibited spontaneous transients even in the absence of ACh application (e.g. D: gray traces; also see: Movie S2. Horizontal Cristae). F) Immunolabeling of a P5 and P6 horizontal canal cristae with the hair cell marker MyoVIIa (green) and neurofilament marker NF200 (blue)

205 show several GAD2-tdT type I hair cells with calyces. Hypothetical clino2 cells and
206 clinocytes cluster near the planum (arrow, P5).

FIGURE S1

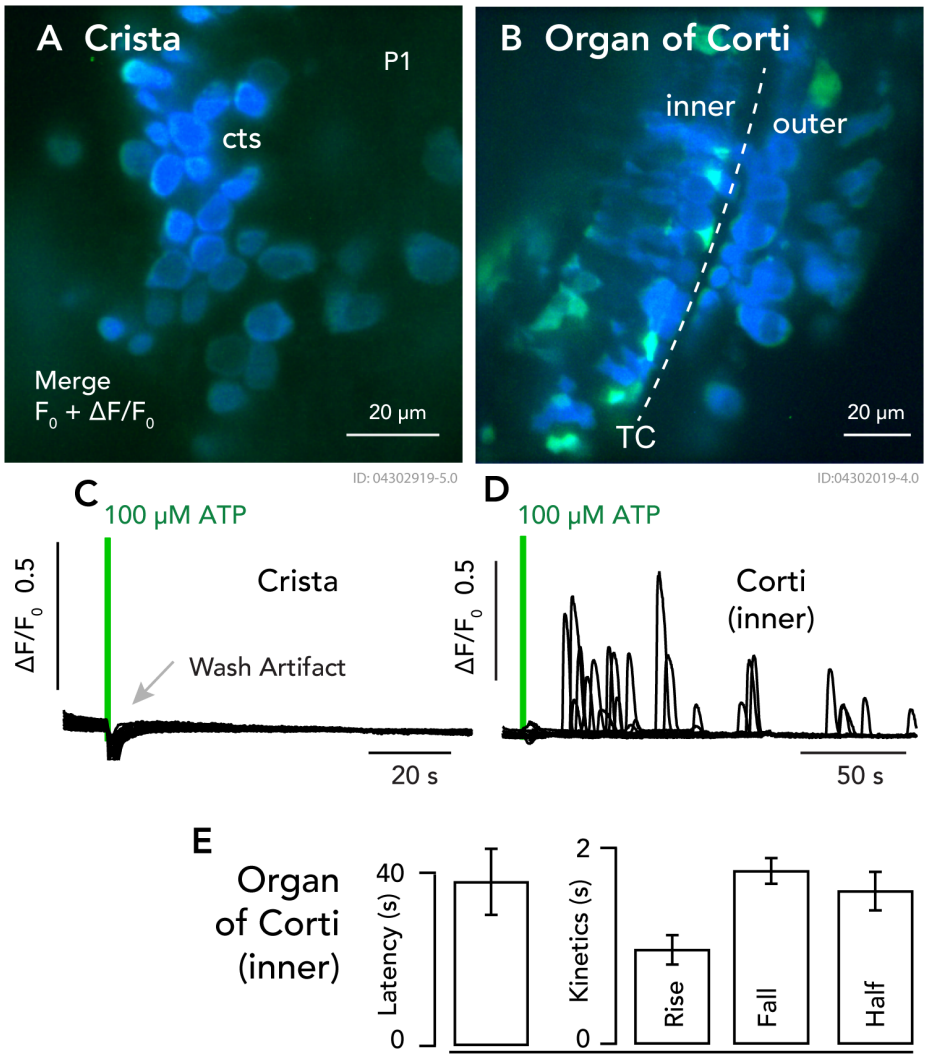
A Crista
P1
cts
Merge
F0 + ΔF/F0
20 μm
B Organ of Corti
inner
outer
TC
20 μm
ID: 04302919-5.0
ID:04302019-4.0
C
100 μM ATP
ΔF/F0 0.5
Crista
Wash Artifact
20 s
D
100 μM ATP
ΔF/F0 0.5
Corti
(inner)
50 s
E
Organ
of Corti
(inner)
Latency (s)
40
0
Kinetics (s)
2
0
Rise
Fall
Half

FIGURE S2

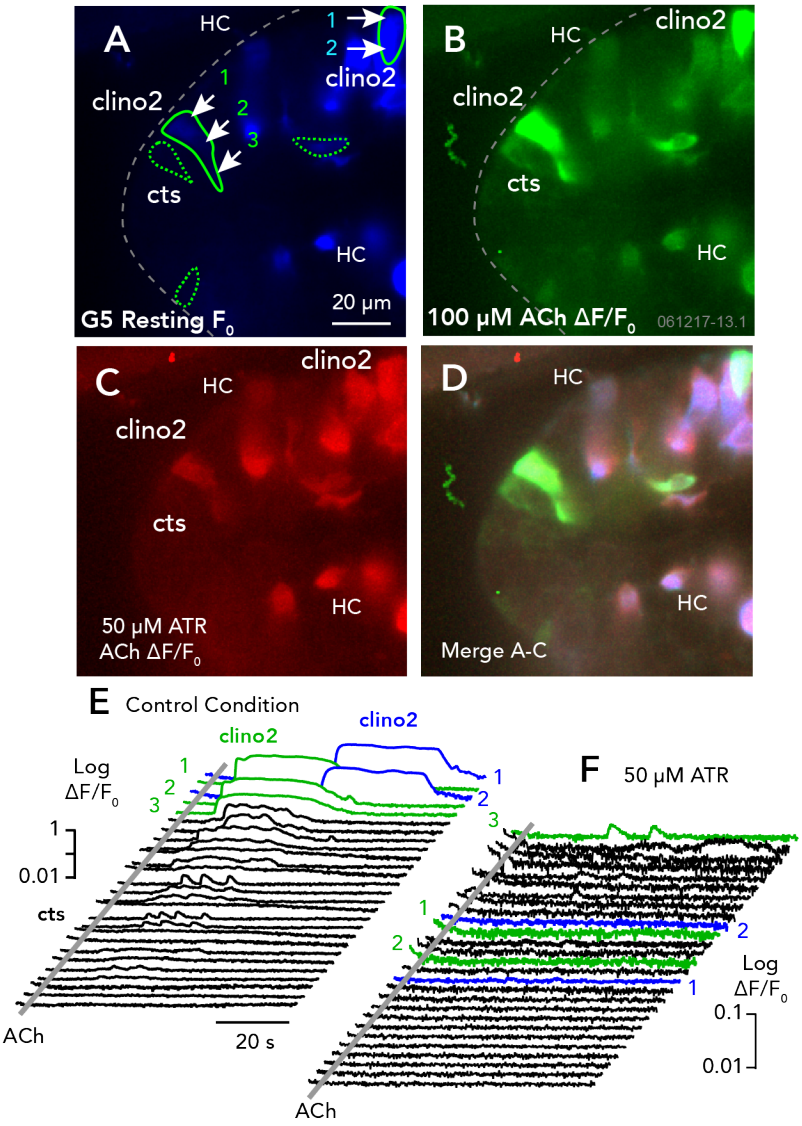

210

211

FIGURE S3

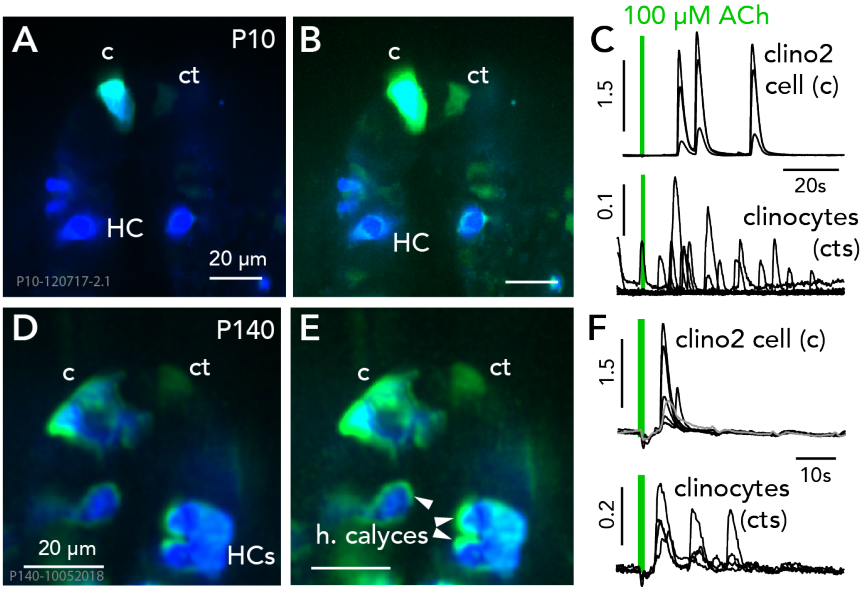

212

213

214

FIGURE S4

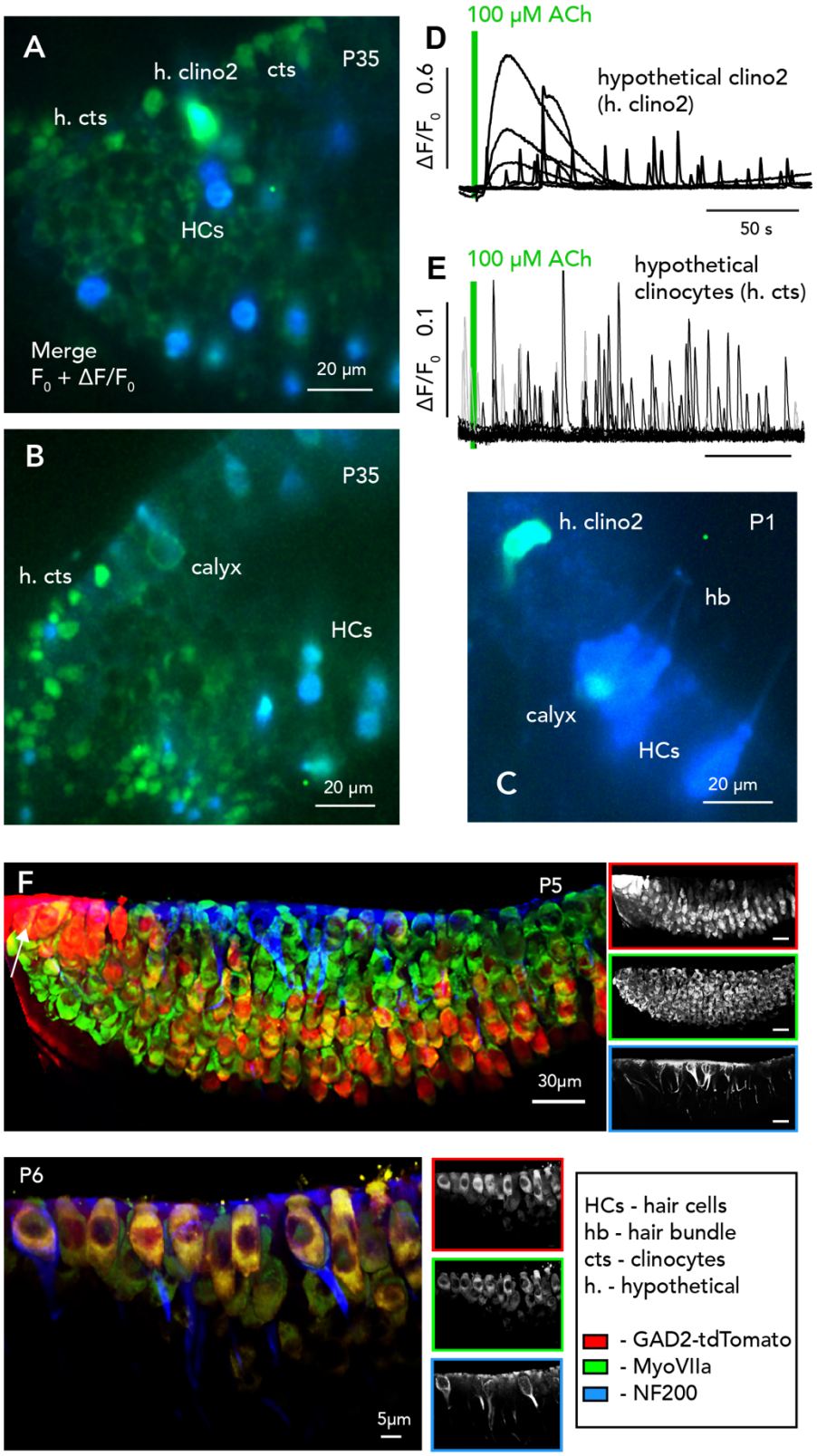

215